condensed matter

MDPI

Review

Probing Phase Separation and Local Lattice Distortions in Cuprates by Raman Spectroscopy

Efthymios Liarokapis

Department of Physics, National Technical University of Athens, 15780 Athens, Greece; eliaro@central.ntua.gr; Tel.: +30-210-7722930

Received: 25 September 2019; Accepted: 27 October 2019; Published: 1 November 2019

Abstract: It is generally accepted that high temperature superconductors emerge when extra carriers are introduced in the parent state, which looks like a Mott insulator. Competition of the order parameters drives the system into a poorly defined pseudogap state before acquiring the normal Fermi liquid behavior with further doping. Within the low doping level, the system has the tendency for mesoscopic phase separation, which seems to be a general characteristic in all high Tc compounds, but also in the materials of colossal magnetoresistance or the relaxor ferroelectrics. In all these systems, metastable phases can be created by tuning physical variables, such as doping or pressure, and the competing order parameters can drive the compound to various states. Structural instabilities are expected at critical points and Raman spectroscopy is ideal for detecting them, since it is a very sensitive technique for detecting small lattice modifications and instabilities. In this article, phase separation and lattice distortions are examined on the most characteristic family of high temperature superconductors, the cuprates. The effect of doping or atomic substitutions on cuprates is examined concerning the induced phase separation and hydrostatic pressure for activating small local lattice distortions at the edge of lattice instability.

Keywords: phase separation; lattice distortions; high temperature superconductors; cuprates; Raman spectroscopy

1. Introduction

Among the most fascinating discoveries over the years is the identification of mesoscopic phase separation (MePhS) in a number of materials, ferroelectrics [1,2], magnetoresistive manganites [3–11], nikelates [12,13], A15 alloys [14], and cuprates [15–52] in which case a spectacular diverse range of exotic magnetic, electronic, and crystal structures can coexist at different locations in the same crystal. In an apparently homogeneous material, it turns out to be surprisingly easy to achieve phase coexistence using a wide range of parameters by playing with the chemical composition or microstructure, increasing an electric or magnetic field, tuning the elastic strain field [53], or by photoinduced phase separation [54,55]. The coexisting phases may form robust magnetic, electronic and crystallographic textures of "mesoscopic" length scales, that is, over tens or hundreds of nanometers. By controlling an array of textured phases, analogous to those in liquid crystals, it is possible to modify locally the electronic structure and properties without atomic-scale fabrication. In manganites for example, a simple domain wall in the ferromagnetic metallic phase could spontaneously develop an insulating barrier of the charge order phase creating the ultimate spin-tunnel junction. Alternatively, in the cuprates, the superconducting domains are separated from an insulating matrix where the thread and the matrix are made of identical material. With these and numerous other ideas for potential applications, one can enter a realm of inorganic material science that is reminiscent of the complex self-organized structures seen in soft condensed matter physics or polymer science.

Structural instability appears in several systems of condensed matter and can play a key role in the characteristic properties of several other compounds (e.g., ferroelectrics), manganites, and high temperature superconductors (HTSC). The role played in the case of HTSC was revealed soon after their discovery [15] by J.C. Philips who correctly pointed out the structural instabilities that accompany either intermetallic or oxide superconductors [56]. For the old superconductors, it had already been found that, in A-15 compounds, structural instability and superconductivity are related [14]. The structural instability actually creates a softening of the lattice and is reflected in several physical properties including the associated phonon modes. In superconductors, the underlying idea of MePhS is that, in the insulator-superconductor transition, the holes introduced in the insulator matrix by the dopant are rejected, forming mesoscopic clusters of the superconducting phase (physical phase separation). The magnetic fluctuations are suppressed in the small dimensions of the randomly oriented clusters and superconductivity is stabilized. The whole process is self-organized, but the metastable phases of the system can be reached by tuning physical variables such as pressure or charge density. Although the mechanism that produces high transition temperature is still unknown, there is general agreement that understanding the normal state where several degrees of freedom (spin, charge, orbital, and lattice) compete, could clarify the situation. It is now well established that, between the Mott insulator and heavy doping charge, ordered states (stripes) are created [12,18] from the competition of the kinetic energy and Coulomb repulsion, but the exact connection of the stripes with superconductivity is not clear yet. It is, therefore, of interest to investigate the responses of the normal state to variations of external factors (temperature or pressure) or internal parameters (doping).

Interest in the role of lattice in the pairing mechanism of HTSC has increased since the discovery of superconductivity with high transition temperature (T_c) [15] in MgB_2 [57–63], the alkali metal doped C60 [64–66], and, more recently, by the very high transition temperature achieved under hydrostatic pressure in sulfur hydrides [67–70]. In the case of cuprates, several experiments (e.g., [71–79]) suggest that phonons play a substantial role in the high Tc mechanism.

Phase separation has been observed using several methods in both pnictides and chalcogenides iron-based superconductors [80–86] and at the insulator to metal transition in VO_2 [87–92]. It has been pointed out that this is generic feature in the proximity of topological electronic Lifshitz transitions [40,51,82] where lattice and electronic effects are both essential and key terms of the physics of these complex quantum phenomena. Therefore, the study of lattice anomalies, such as soft modes or structural instabilities, is of central interest in the investigation of the HTSC.

Raman spectroscopy is one of the tools used for investigating the characteristics of the new compounds and for providing important information on the carriers through their coupling with the phonons [93], the appearance of new phases [94,95], the anharmonic coupling of the phonons [96–98], the existence and the size of a gap [99], its symmetry [100], and on crystal field excitations [101], etc. In this review, cumulative results from our systematic micro-Raman studies on two families of the cuprates (yttrium and lanthanum families) are presented. Our studies on other high T_c compounds, such as the diborides [60,62,63,102] and the pnictides [103–105] not presented here, have shown similar results with the cuprates. The role of doping, atomic substitutions, and hydrostatic pressure are examined in detail for creating phase separated domains and structural instabilities. It should be noted that our spontaneous Raman studies cannot discriminate between static and dynamic phase separated effects, and it detects them as statistically distributed in space domains.

2. The Yttrium Family Cuprates

Detailed analysis of the lattice vibration symmetry of $YBa_2Cu_3O_x$ can be found in numerous publications (see e.g., [106]). The compounds have an approximate tetragonal symmetry with a small orthorhombic distortion in the superconducting phase [107]. Because of the center of inversion, the zone-center optical phonons are either Raman or IR active. The atoms of the chains (O_{ch}, Cu_{ch}) and Y have full point group site symmetry being IR-active ($B_{2u,3u}$ and B_{1u}), Ba, and apical oxygen (O_{ap}). The CuO_2 plane atoms (Cu_{pl}, O_{pl}) have lower symmetry (C2) and they participate in three phonons of

even symmetry A_g, $B_{2g,3g}$ and three phonons of odd symmetry B_{1u}, $B_{2u,3u}$ (along the c, a, and b axis, correspondingly). The main difference between the orthorhombic and the tetragonal phase are the out-of-phase vibrations of O_{pl} atoms, which in the former case have the A_g symmetry and in the latter case, B_{1g} symmetry, and can be easily identified from the distinct polarization selection rules [106]. Characteristic Raman spectra are shown in Figure 1a,b for the y(cc)y and y(xx)y scattering geometries and the strong Raman active phonons of A_g symmetry along the c-axis for $YBa_2Cu_3O_{7-\delta}$ are located at ≈116 cm^{-1} (Ba), ≈150 cm^{-1} (Cu_{pl}), ≈435 cm^{-1} (in-phase vibrations of O_{pl} atoms), and ≈502 cm^{-1} (O_{ap}).

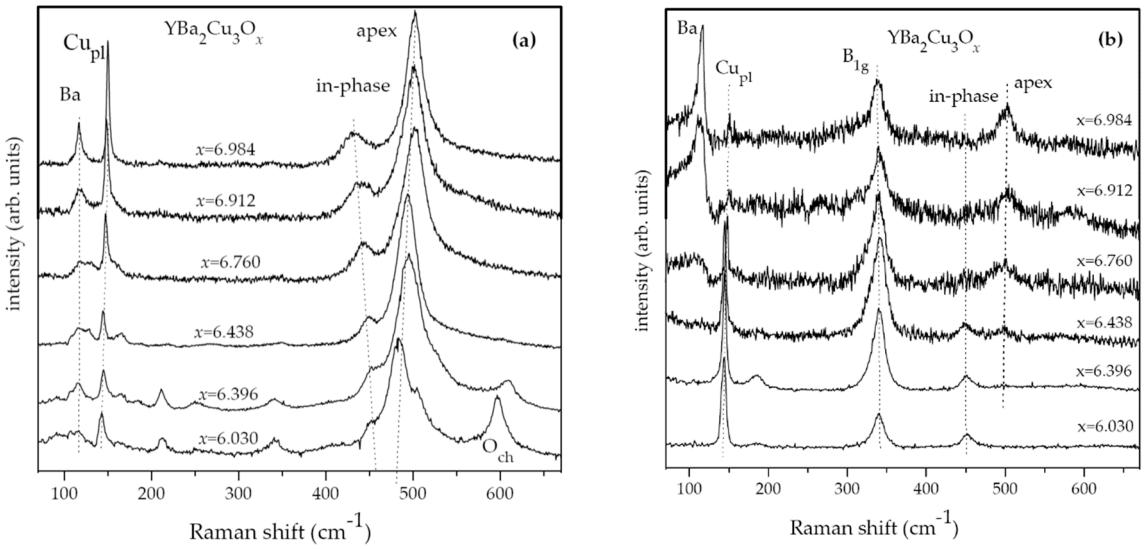

Figure 1. Typical spectra of $YBa_2Cu_3O_x$ at room temperature using the 514.5 nm laser line in the y(cc)y (**a**) and y(xx)y (**b**) polarization.

2.1. Phase Separation from Oxygen Doping

The A_g symmetry strong modes due to the Ba and Cu_{pl} atoms vary considerably in intensity with oxygen concentration in the y(xx)y scattering configuration (Figure 1b) and Ba phonon has a strong asymmetric shape that gradually disappears in the tetragonal phase ($x \leq 6.35$). The Cu_{pl} phonon shows the opposite behavior, being very weak in the fully oxygenized compounds ($x \approx 7$) and gaining intensity by the orthorhombic to tetragonal (O-T) phase transition (Figure 1). In the y(cc)y scattering geometry, these phonons appear in all oxygen concentrations without considerable intensity variations (Figure 1a). In this scattering geometry, the Ba phonon is symmetric, which indicates that the asymmetry observed in the other geometry is due to its coupling with the carriers. Its intensity is modified by the amount of oxygen which reflects the carrier redistribution with doping between the BaO and the CuO_2 planes. At low doping, the carriers are distributed outside the CuO_2 planes screening the Ba phonon, which appears with very low intensity (or it is completely absent) in the xx scattering polarization. Exactly the opposite happens to the Cu_{pl} phonon, which is strong at low carrier concentrations and disappears with increasing doping. As carriers are transferred to the CuO_2 planes they induce strong screening of the Cu_{pl} phonon, while the Ba mode gains intensity (Figure 1b).

Oxygen nonstoichiometry is the crucial parameter controlling such a diverse behavior for the compound as one follows the transition from $YBa_2Cu_3O_6$ to $YBa_2Cu_3O_7$. It is, therefore, natural to concentrate on the oxygen Raman active modes. The dependence of the O_{ap} mode energy on the oxygen concentration is nonlinear [107]. Roughly described, the energy remains almost constant in the range of $6.75 < x < 7.00$, is reduced in the range of $6.15 < x < 6.75$, and, finally, for $x < 6.15$, there is a sudden drop in frequency (Figure 2a). The mode linewidth exhibits the following three minima: for maximum x values, for $x \approx 6.47$, and in the range of $x < 6.12$. Contrary to early Raman spectra, which have shown a linear dependence of its energy with the amount of oxygen [108], the results in Figure 2 show that it remains practically constant in the range of $6.8 < x < 7.0$ and, then, decreases

with decreasing x (Figure 2a). More pronounced changes appear in the width of this phonon with a maximum close to x = 6.7 and then a decrease towards the two ends (Figure 2a), which is a result of the appearance of new phases, as discussed below.

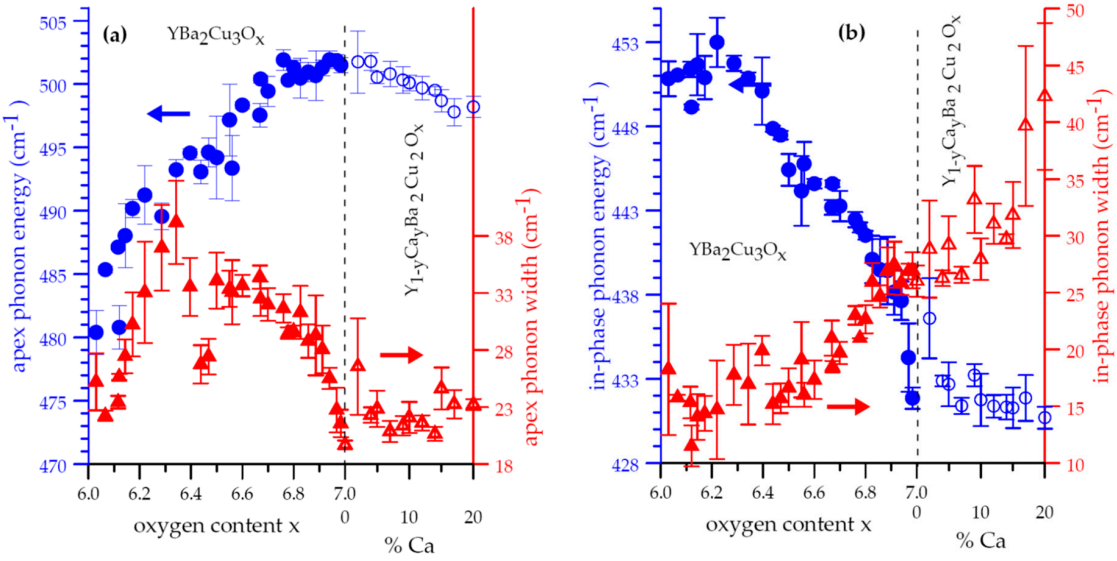

Figure 2. Apex (**a**) and in-phase (**b**) phonon energy and width dependence on amount of oxygen content for $YBa_2Cu_3O_x$. Corresponding data for $Y_{1-y}Ca_yBa_2Cu_3O_{7-\delta}$ are presented with % amount of Ca. Error bars indicate statistical distribution of data from various microcrystallites.

In the $YBa_2Cu_3O_x$ (Y123x) compounds, Cu atoms also exist outside the CuO_2 planes, forming linear chains along the b-axis. As the rest of the HTSC does not have such chains, it is believed that they do not play a crucial role in superconductivity, although they influence the properties of the Y123x system. In the fully occupied chain (Y1237), all oxygen atoms are, in principle, located along the b-axis, and, as the number of oxygen atoms is decreased, there is always a tendency to form thermodynamically stable structures [109]. Two such phases with T_c at 60 K (ortho-II, for $x \approx 6.5$), which correspond to alternating full and empty chains, and at 92 K (ortho-I, fully oxygenated samples) are well established appearing as characteristic plateaus in the phase diagram [110]. For lower concentrations ($x \leq 6.35$), a transition takes place to an antiferromagnetic, non-superconducting phase [107]. The exact stoichiometries, where the phases appear, depend on the preparation conditions [107]. This is due to the existence of many other intermediate phases, which correspond to different combinations of full and empty chains that are examined below. Such ideal ordered microstructures can only be stabilized after a careful annealing of the materials; otherwise the disorder will make the compound appear macroscopically tetragonal [111]. The changes induced in the chains from the removal of oxygen, have a direct effect on the position of the apical oxygen, which moves away from the superconducting CuO_2 planes [110]. In terms of the valences, this is an indication of redistribution of charges between the chains and the planes as oxygen is added in the system [100]. Another way to explain the phase transformation from the antiferomagnetic to the superconducting state was proposed within the phase separation model [112]. As oxygen atoms are added, and holes are transferred to the CuO_2 planes, conducting microdomains are formed, which, when there are enough, are connected and the system becomes a superconductor. A further increase of holes in the planes induces another phase transition with higher T_c (92 K). The appearance of these phases is connected with the distribution of the oxygen atoms in the chains along the b-axis forming two- or three-dimensional superlattices [109]. Some of these structures have been observed (tetragonal, ortho-II, and ortho-III phases) and they correspond to $x \approx 6$, $x \approx 6.5$, and $x \approx 6.67$ [109–111]. The effect of the removal of the chain oxygen on the Raman spectra is shown in Figure 1. As discussed above, on the one hand, the relative intensity of the low frequency modes (Ba and Cu_{pl}) depends strongly on the amount of oxygen (mainly in the y(xx)y scattering

geometry), but their energy is not modified appreciably. On the other hand, the oxygen content affects very strongly both the energy and width of the apical oxygen and the in-phase phonons (Figure 2). This is due to the appearance of new phases, as resonance examination of these oxygen modes in the excitation energy range of 1.6–2.9 eV, for the tetragonal and orthorhombic Y123x system, has revealed [113]. Concerning the A_g symmetry apical oxygen phonon, it has been found to show a strong resonance in the IR excitation for the tetragonal case, with additional modes appearing, which are absent when the excitation is in the visible region of spectrum [114]. Work carried out by Iliev et al. [94] has shown a very characteristic variation of the apical A_g phonon when the excitation wavelength varied from blue (482.5 nm) to red (647.1 nm) for the $YBa_2Cu_3O_{6.4}$ compound. Our investigations confirmed this by showing that, in the fully oxygenated ortho-I phase, the O_{ap} mode does not shift with varying excitation wavelength (Figure 3a) and it is modified considerably for the underdoped compound (Figure 3b) due to the different cross sections of the coexisting phases, with the lower T_c phases being in resonance with lower energy excitations [113,114].

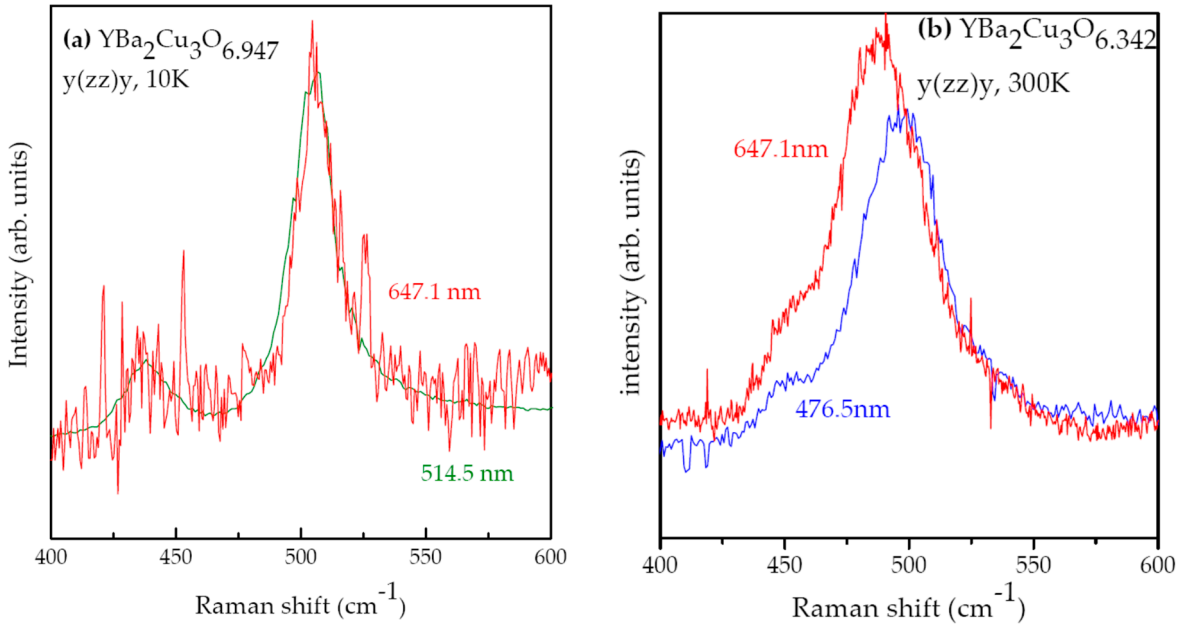

Figure 3. Apex and in-phase oxygen modes excited with various laser lines for optimal doped (**a**) and underdoped (**b**) compounds.

Other measurements also suggest the coexistence of phases [115]. Since the apical oxygen mode is very sensitive to the chain ordering [93,116] and its width shows minimum values around $x \approx 6$, $x \approx 6.47$, and $x \approx 7$ (Figure 1a), one could assume that at least three phases are present. But the resonance measurements have revealed the existence of four peaks located at 502 cm^{-1}, 493 cm^{-1}, 486 cm^{-1}, and 476 cm^{-1} that correspond to four coexisting phases. The higher and the lower energy peaks certainly correspond to ortho-I and the tetragonal $x \approx 6$ phases. From our measurements and other measurements on $x \approx 6.5$, it is clear beyond any doubt that the 493 cm^{-1} is a superstructure peak due to the ortho-II phase (doubling of unit cell with half occupation of the chains). In order to delineate the origin of the 486 cm^{-1} peak, we consistently carried out a deconvolution of all Raman spectra from 30 samples of varying oxygen concentrations with ^{16}O and 23 samples with ^{18}O, and the results are presented in Figure 4 (similar results exist for ^{18}O in [98]). It appears that the 486 cm^{-1} peak corresponds to a phase in the tetragonal doping region. From the similarity in energy, the superstructure (S) peak at 486 cm^{-1} could correspond to the breathing (0.5, 0.5, 0) mode [117], but then it should peak around $x \approx 6.25$, contrary to the deconvolution results (Figure 4). A better guess is the $2\sqrt{2}a_o \times 2\sqrt{2}a_o \times c$ diagonal superlattice phase based on the amount of oxygen [118–120]. In order to extract more information from the Raman spectra, as shown in Figure 5, we plotted a histogram of

the peak positions for the apex and in-phase modes. A preference appears for certain wavenumbers, which correspond (from Figure 2) to the phases indicated in Figure 5. The ortho-I and ortho-II phases are clear, while the superstructure S peak seems to correspond to x ≈ 1/8 (2 $\sqrt{2}a_o \times 2\sqrt{2}a_o \times c$) phase. Furthermore, there are indications of other phases for wavenumbers pointing to an ortho-III (x = 6.67) or even higher phases [121]. In a systematic imaging of the spatial ordering of the oxygen chains in $YBa_2Cu_3O_{6+y}$, by micro X-ray diffraction measurements, the phase separated regions have been detected [122–124]. For y = 0.33, the ortho-II phase was clearly detected embedded in more disordered regions [124]. For y = 0.67, nano-puddles corresponding to y = 0.5 + 1/8 were found corresponding to the ortho-VIII puddles of alternating five filled and three empty oxygen wires every eight rows [122]. Other networks were created by thermal manipulation [123]. Unfortunately, no Raman data exist on the same compounds for comparison, but our studies agree with these results and at least the one-eighth oxygen ordering seems to be a preferential oxygen ordering for both the $YBa_2Cu_3O_6$ and the $YBa_2Cu_3O_{6.5}$ stable phases. Furthermore, the regions assigned to OIII phase in Figure 5 possibly consist of several other phases similar to the ones discovered by X-ray imaging [122,123]. This can explain the less pronounced nature of the OIII peaks in Figure 5 for both the apex and the in-phase modes. Finally, there is another peak in the overdoped region, as strongly indicated from the in-phase mode and discussed below.

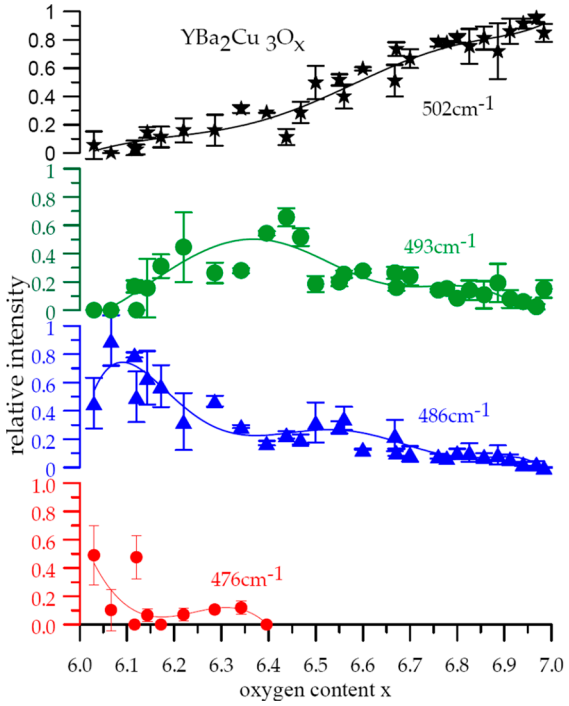

Figure 4. Relative amounts of coexisting phases in $YBa_2Cu_3O_x$ compound at different doping levels.

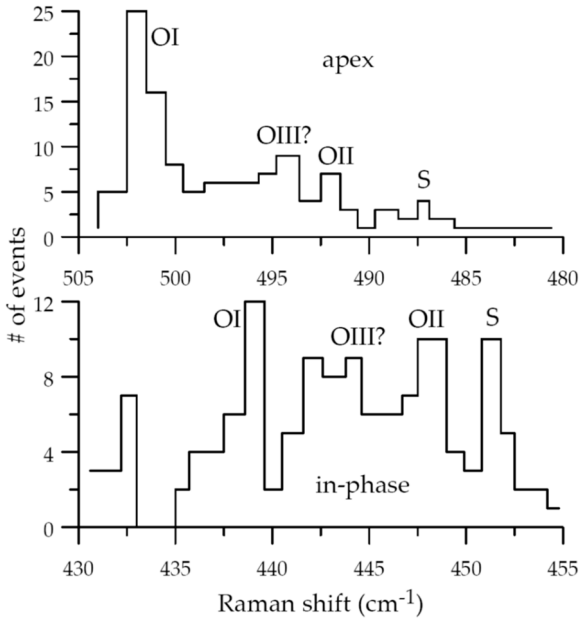

Figure 5. Histograms of apex and in-phase peak positions of $YBa_2Cu_3O_x$ showing various phases.

As seen in Figure 2b, the in-phase O_{pl} mode energy and linewidth values remain constant in the range of $6.00 < x < 6.40$. At higher doping levels, the energy monotonically decreases, while the linewidth increases almost linearly and, finally, it softens by ~8 cm^{-1} close to optimal doping (Figure 2b). An analysis of the Raman measurements shows that microcrystallites of the two different phases could be found within the same compound with the in-phase phonon energy either corresponding to the optimally or the overdoped concentration. This is the reason for the increased error bars (the statistical distribution from measurements from several microcrystallites) for the overdoped data of in-phase phonon energy in Figure 2b. The EXAFS [125] and neutron [126] scattering measurements have shown that, at exactly this oxygen concentration, there is a sudden modification in the buckling of the CuO_2 planes with a reduction in T_c [127]. Apparently, this softening is related to the change in the buckling. Therefore, we conclude that two phases coexist for $x \geq 6.94$ and only the relative amount of each phase varies with oxygen content [127]. It should be stressed that the miscibility gap, seen as a split-off peak below 435 cm^{-1} in Figure 5 (in-phase mode), is observed even between microcrystals of the same sample, i.e., $x = 6.940$. This fact underlines the martensitic character of the phase transition. A similar softening has been observed for the ^{18}O samples [98], and in samples where the La has been substituted in half by another rare earth ($La_{0.5}R_{0.5}Ba_2Cu_3O^x$) [128], but not in the homologous series $Pr_{0.5}R_{0.5}Ba_2Cu_3O_x$ [129]. It has been shown that the softening is not related to the amount of doping, as the alternative way of doping by Ca substitution ($Y_xCa_{1-x}Ba_2Cu_3O_y$) does not induce such a softening ([130] and following session). As La has the tendency of attracting more oxygen atoms, the softening must be attributed to structural modifications induced by the excess of oxygen atoms.

2.2. *Phase Separation from Atomic Substitutions*

The B_{1g} mode is sensitive to atomic substitutions for yttrium and its broadening was used to measure the superconducting gap by tuning the phonon energy across the gap energy for carefully chosen rare earth substitutions [131]. By studying a series of rare earth substitutions, $La_{0.5}R_{0.5}Ba_2Cu_3O_{7-\delta}$ [128], $R_{0.5}Pr_{0.5}Ba_2Cu_3O_{7-\delta}$ [129], $Y_{1-x}La_xBa_2Cu_3O_{7-\delta}$ [132], and $Y_{1-x}Pr_xBa_2Cu_3O_{7-\delta}$ [133], it has also been found that the B_{1g} mode splits into two or three bands, depending on the difference of the atomic radii of substituting species and this is related to the superconducting property. On the one hand, in all these cases, the XRD studies could not discriminate more than one component, although modifications in the interatomic distances at critical differences of the ion size have been found [128]. This indicates that any phase separation in those systems

occurred at distances smaller than the coherence length of XRD. On the other hand, Raman measurements with smaller coherent length could clearly detect the multiphase structure of the compounds [128,129,132,133]. Characteristic spectra for the evolution of the strong modes with rare earth substitution for $Y_{1-x}La_xBa_2Cu_3O_{7-\delta}$ are shown in Figure 6 [132]. Similar Raman spectra have been found for the other substitutions [128,129,133].

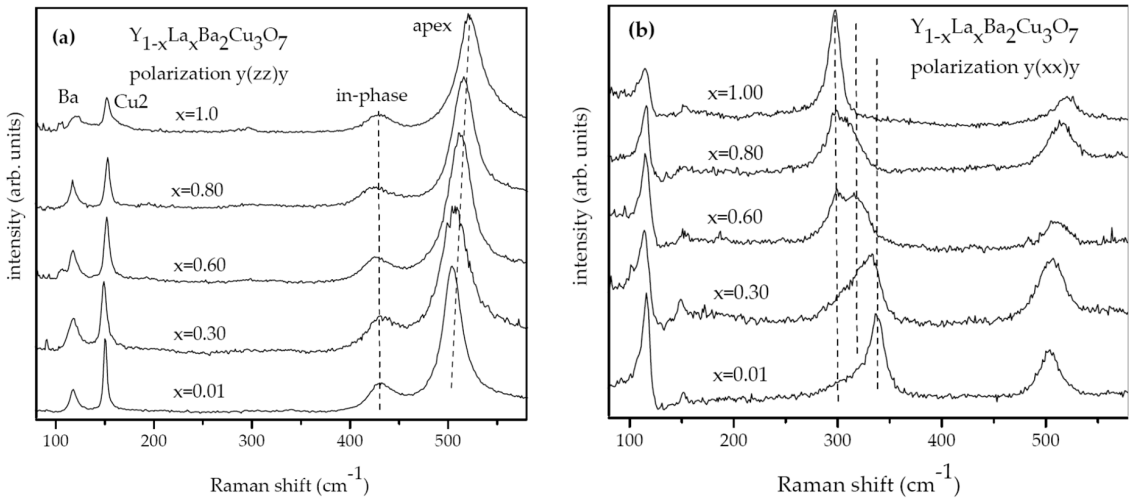

Figure 6. Raman spectra from selected La concentrations for polarizations along the c-axis (**a**) or the ab-plane (**b**).

Concerning the other modes, the apex oxygen mode in Figure 6 shifts continuously depending on the average ionic radius of the substituting rare earth elements, in agreement with the results from the system $RBa_2Cu_3O_{7-\delta}$ [134]. The in-phase mode is more or less insensitive to rare earth (Figure 6), although there might be variations, as much as 7 to 8 cm^{-1}, if the oxygen content varies slightly below or above the optimal doping value (Figure 6). In addition, the Cu_{pl} phonon is not modified by the substitution. The Ba phonon also does not vary in energy, but its intensity has been strongly quenched in the xx polarization by Pr substitution [128,129], which is due to the partial substitution of Pr for Ba, explaining the unexpected strong reduction in T_c in that case [133]. The most sensitive is the B_{1g} mode that follows one- or two-mode behavior [135] depending on the radius difference of the two atoms [128,129]. As seen in Figure 6b, this phonon splits into two or three bands, which apparently correspond to the end members and an intermediate one. In the case of $Y_{1-x}Pr_xBa_2CuO_{7-\delta}$, the transition temperature decreases as Pr substitutes for yttrium up to 60%, and above that, the compound does not superconduct (Figure 7). Plotting the relative amount of the various phases as induced by the B_{1g} phonon mode, it is observed that T_c does not follow the evolution of the relative amount of the intermediate mixed state, which is the leading phase up to 80% Pr content, where the compound is not superconducting (Figure 7). This is proof that both the pure Pr123 ($Y_{1-x}Pr_xBa_2CuO_{7-\delta}$) and the intermediate mixed phases are not superconducting and the superconductivity in these compounds is only due to the percolation via the Y123 ($YBa_2Cu_3O_{7-\delta}$) phase.

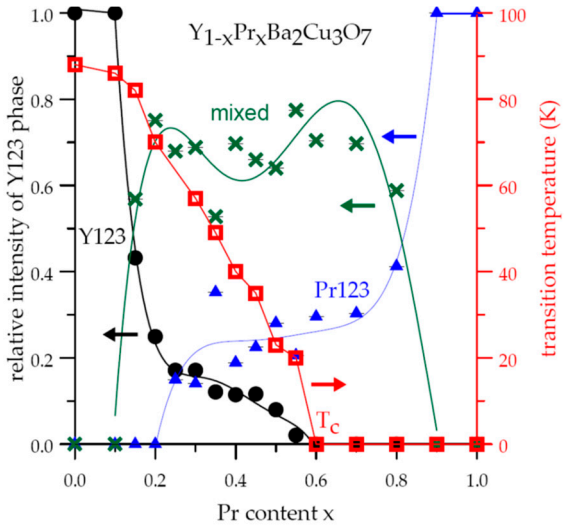

Figure 7. Relative intensity of the three phases as obtained from the B_{1g}-symmetry phonon.

Because, in YBa_2CuO_x, there is no way to add more oxygen beyond x = 7, overdoping can be achieved by Ca substitutes for yttrium. This substitution has two effects; an increase of holes creating overdoping, and creation of strains from the size difference between the Ca and Y ions. Furthermore, the local electric field in the CuO_2 planes from the Y/Ca and Ba sites is modified, which could possibly affect the phase separation observed in the rare earth substitutions for yttrium [128,129]. The results of the Ca substitution on the strong phonon modes for the y(xx)y scattering polarization are shown in Figure 8. The A_g-symmetry modes, due to Ba and Cu2, are not modified considerably by the Ca substitution (Figure 8) implying that Ca does not substitute for isovalent Ba. The relative intensity of the Cu2 to Ba in the xx polarization is also not modified because the excess doping continues screening the Cu2 atoms [130]. In the Ca substitution for the Y overdoped region, the energy of the O_{ap} phonon decreases (Figure 2a) following the bell-shaped trend of T_c. The width of the phonon remains close to its value for the ortho-I phase (Figure 2a), verifying that the substantial increase in the width with oxygen doping in pure $YBa_2Cu_3O_x$ is due to the ordering of the chain oxygen atoms.

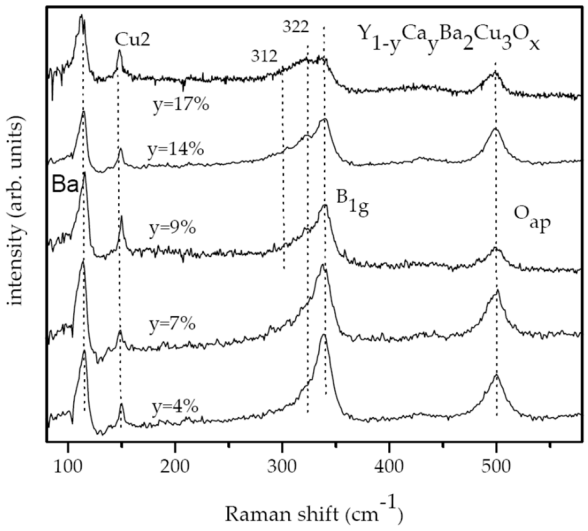

Figure 8. Raman spectra of $Y_{1-y}Ca_yBa_2Cu_3O_x$ for the y(xx)y scattering polarization.

Figure 9 shows that the decrease in energy of the apical oxygen mode is due to the increase in the distance of the O_{ap} from the CuO_2 planes. Apparently, the extra carriers introduced in the CuO_2 planes from the Ca substitution induce redistribution of charges between CuO_2 planes and CuO chains

repelling the apical oxygen from CuO_2 planes. Although the data are limited, it seems that there is a stepwise increase in the CuO_2-O_{ap} distance with Ca overdoping. Since the accurately measured amount of oxygen does not vary appreciably with Ca substitution (Figure 10) and the width of the apex mode is almost the same as for the ortho-I phase (Figure 2), this effect could not be due to coexisting phases from chain ordering. Possibly, it indicates the tendency of O_{ap} to stay at discrete positions along the c-axis as in a double well potential, or equivalently discrete charge transfers from chains to the superconducting planes. Such an important effect requires further investigation using several Ca concentrations and fully oxygenated samples.

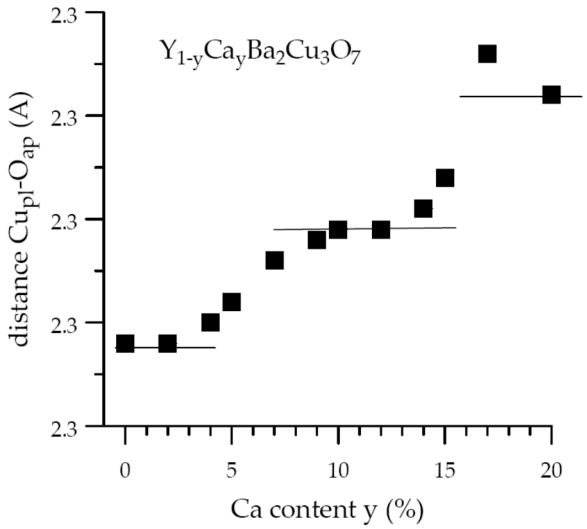

Figure 9. Modification of the Cu_{pl} and O_{ap} distance in Å for the $Y_{1-y}Ca_yBa_2Cu_3O_x$ compound.

The in-phase vibrations of O_{pl} atoms are strongly dampened by oxygen doping, with their energy reducing and the width increasing with x in pure Y123x compound (Figure 2b). The overdoping with Ca further increases the width and to a lesser degree decreases the energy (Figure 2b), although the presence of the phonon softening at oxygen overdoping complicates the effect. The relative amount of the softened phase located at 428 cm^{-1} in the Ca substituted compounds to the total counts of in-phase mode, correlates very well with the amount of oxygen and not with the concentration in Ca (Figure 10). The EXAFS measurements have indicated that the carriers introduced by Ca do not reside at the CuO_2 (or the BaO) planes, but the Ca atoms act as pinning centers for these excess carriers [136]. In such a case, the continuous reduction in T_c with the amount of Ca could be a result of percolation from the separation into at least two phases (Figure 8), a pure $YBa_2Cu_3O_{7-\delta}$ and a mixed one not superconducting. In the studies of the $R1_{1-x}R2_xBa_2Cu_3O_{7-\delta}$ systems, we have observed that the B_{1g}-mode splits into two or three modes that correspond to two end compounds and a mixed phase. In the Ca case, in addition to the B_{1g}-symmetry mode of $YBa_2Cu_3O_{7-\delta}$ which is gradually reduced in intensity with the amount of Ca, another mode of A_g-symmetry at ≈322 cm^{-1} appears to gain intensity with the substitution, but its energy remains unaffected by the amount of Ca. This extra mode must correspond to the mixed phase. On the basis of the B_{1g} phonon energy dependence on the ion size [128,129,132], we can deduce that it could roughly correspond to a $Y_{0.5}Ca_{0.5}Ba_3O_{7-\delta}$ phase.

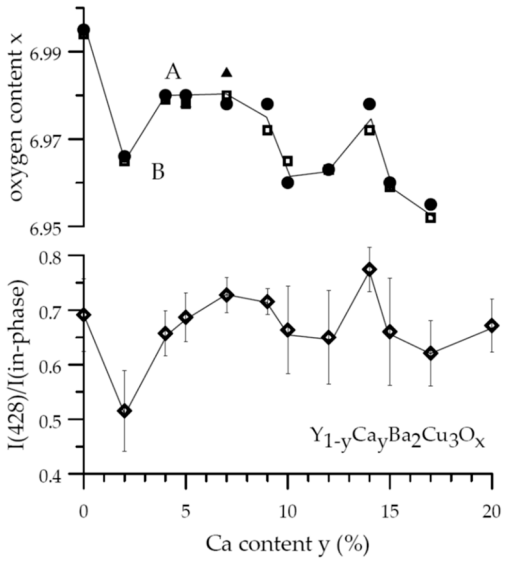

Figure 10. Relative intensity of 428 cm^{-1} mode and its correlation with amount of oxygen.

Furthermore, there is a very weak mode at ≈312 cm^{-1} activated by the Ca substitution (Figure 8). In the pure $YBa_2Cu_3O_7$ system, there is a mode of $B_{2g,3g}$ symmetry due to vibrations of the yttrium ions. The substitution of heavier yttrium atoms by Ca should induce a shift of ≈5% in frequency as compared with the 10% difference observed. It is, therefore, unlikely that the two modes are related and most likely the ≈312 cm^{-1} mode corresponds to an ideal $CaBa_2Cu_3O_x$ phase, which is unstable as a free compound.

2.3. Pressure Induced Lattice Effects

As detected by the softening of the in-phase mode (Figure 2b) and confirmed by other measurements [125,126], $YB_2Cu_3O_{7-\delta}$ at optimal doping with maximum T_c is at the edge of a lattice instability undergoing a small lattice distortion. Systematic Raman studies on various high Tc cuprates have revealed nonlinear lattice distortions and lattice instabilities induced by the application of hydrostatic pressure [137–141], which correlate with the non-monotonic pressure dependence of T_c. This is not surprising because it is well accepted that structural and electronic inhomogeneities constitute intrinsic properties of cuprate superconductors [10,142,143]. The Raman study of hydrostatically compressed $YBa_2Cu_3O_y$ (Y123x) and $YBa_2Cu_4O_8$ (Y1248) cuprates revealed deviations from an expected linear behavior in the phonon characteristics indicating lattice instabilities [139,144] at those pressures where T_c dependence shows saturation or nonlinear behavior [145,146]. Synchrotron angle-dispersive powder diffraction measurements with dense sampling on optimally doped Y1237 and Y1248 [147] superconductors verified the Raman results showing clear deviation of the lattice constants from the expected equation of states (EOS) followed by a strong hysteresis effect in the same pressure range, which disappear in the non-superconducting $PrBa_2Cu_3O_7$ (Pr1237) [147].

Figure 11 presents the comparative results on the hydrostatic pressure dependence of the lattice parameters a, b, and c for the three compounds (superconducting Y1237, Y1248, and non-superconducting Pr1237). At the bottom of the figure, the corresponding relative strain is depicted for the three cases. Full symbols correspond to the measurements to increase the pressure and open symbols for those obtained on pressure release. It was found, as expected, that the compressibility along the a-, b-, and c-axis is anisotropic, with the c-axis exhibiting the strongest reduction upon pressure [147]. The main result is the strong deviation of the pressure dependence of the c-axis that starts around 3.7 GPa and extends to 8 to 10 GPa (Figure 11). The deviation also exists in the same pressure range for the other two axes, but it is much smaller. It is interesting that there is a substantial hysteresis effect with the data following the decompression the expected EOS. The nonlinear

evolution of the lattice constants, with the applied pressure, originates from similar modifications in the interatomic distances such as the Ba distance from the basal plane, the Cu2-O_{pl} bond length, and the Cu2-Cu1 distance along the c-axis [147]. Concerning the relative strain calculated from the (113) line, it shows three pressure regions (Figure 1, bottom). Up to ~3 GPa, the data among the three compounds agree following the expected slight increase in the line width and, in the region ~3 to 8 GPa, there is a change in the slope only in the two superconducting compounds (Y1237 and Y1248) to be followed by a further increase in slope at higher pressures, which is common in all three cases. It seems that at the critical pressure range of ~3–8 GPa, something happens to the lattice which affects the carriers related to superconductivity. Above ~8 GPa, there must be another effect which is common to all compounds.

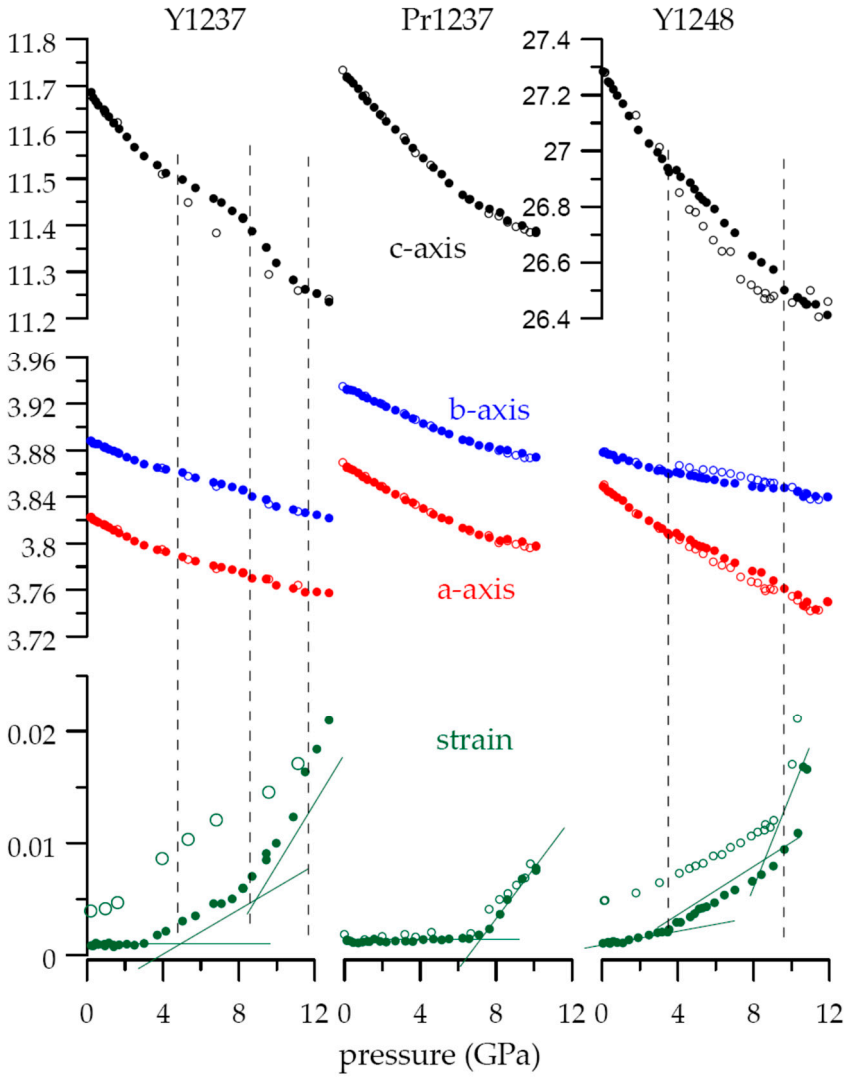

Figure 11. Pressure dependence of the lattice constants (a-, b-, and c-axis) and lattice strain (bottom graphs) for $YBa_2Cu_3O_{7-\delta}$ (Y1237), $PrBa_2Cu_3O_{7-\delta}$ (Pr1237), and $YBa_2Cu_4O_8$ (Y1248) compounds. Full (empty) symbols for increasing (decreasing) pressure.

Figure 12 presents the comparative results of Raman measurements among superconducting Y1237 and non-superconducting Pr1237 for the strong A_g-symmetry phonons that involve the O_{ap}, $O_{in\text{-}ph}$, Ba, and Cu2 atoms. The clear anomaly and the plateau around 3 GPa observed in Y1237 is absent for Pr1237 and the results agree with the X-ray diffraction measurements (Figure 11) and the modifications in the interatomic distances [147]. Raman data have shown that, even for the ortho-II

phase, a similar anomaly exists in the A_g-symmetry phonon modes [147]. Although no hydrostatic Raman pressure data exist for the Y1236 compound, the absence of this anomaly for Pr1237 supports the hypothesis that this effect is related with the carriers.

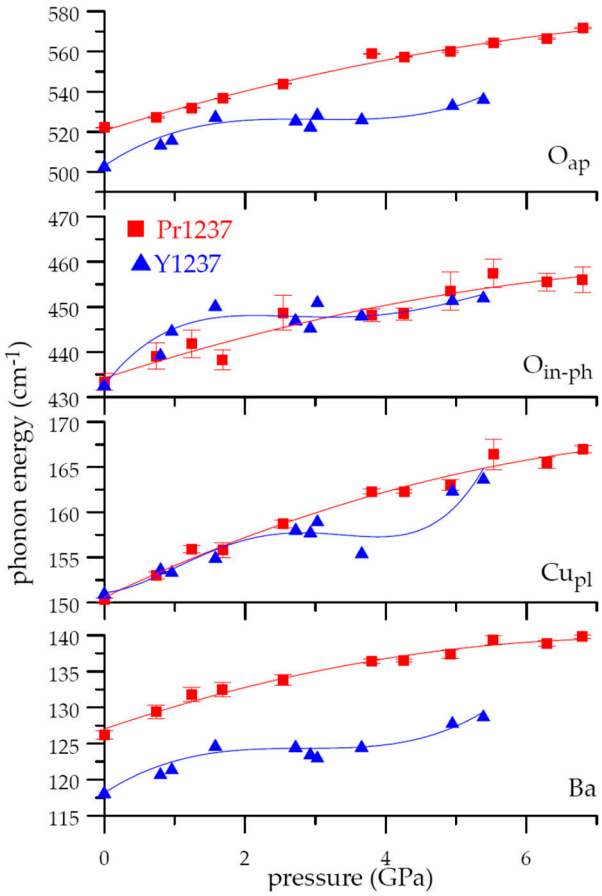

Figure 12. Room temperature pressure Raman data for the A_g-symmetry phonons of the $YBa_2Cu_3O_{7-\delta}$ (Y1237, triangles) and $PrBa_2Cu_3O_{7-\delta}$ (Pr1237, squares) systems.

The c-axis modification with pressure is a result of interatomic bond length changes resulting from pressure-induced charge redistribution or internal strains in the structure. Charge redistribution among the planes has been found to occur in the case of chemical pressure [148] affecting T_c and must certainly play some role in the observed effects. The correlation of the structural characteristics with Raman spectral modifications of the in-phase O_{pl} and O_{ap} phonon modes (Figure 12) and corresponding changes of T_c [145,146] imply that the trigger of the lattice instabilities lies among the CuO_2 and BaO planes. The average Cu2-O_{pl} bond distance is almost constant in the low pressure region, up to ~1.5 GPa, it decreases for increasing pressure up to 3.7 GPa, remains almost constant in the range of 3.7 GPa < p < 8 GPa, and decreases further for p > 8 GPa [149]. The fractional coordinate z of the Ba atom along the c-axis also shows similar modifications at the same pressures (Figure 13, bottom). In the low-pressure region, up to ~1.5 GPa, the fractional coordinate z of Ba decreases almost linearly with pressure. With increasing pressure, z increases and levels off for 3.7 GPa < p < 8 GPa, indicating that the Ba atom moves away from the basal plane. For p > 8 GPa, z is decreasing indicating that Ba atom is again pushed towards the basal plane. Upon pressure release, the movement of the Ba atom clearly shows a hysteresis effect (Figure 13). The Cu2-Cu1 distance in the perovskite block hosting the Ba atom shows similar deviations from linear behavior at the same pressures (3.7 GPa and ~8 GPa, top of Figure 13). Since this distance is related to the transfer of carriers from the CuO chains to the CuO_2 superconducting planes, its abnormal modification with pressure is certainly connected with an

irregular transfer of carriers to the CuO_2 planes. Therefore, the data point to lattice instability at a critical pressure, which affects the carrier distribution and T_c.

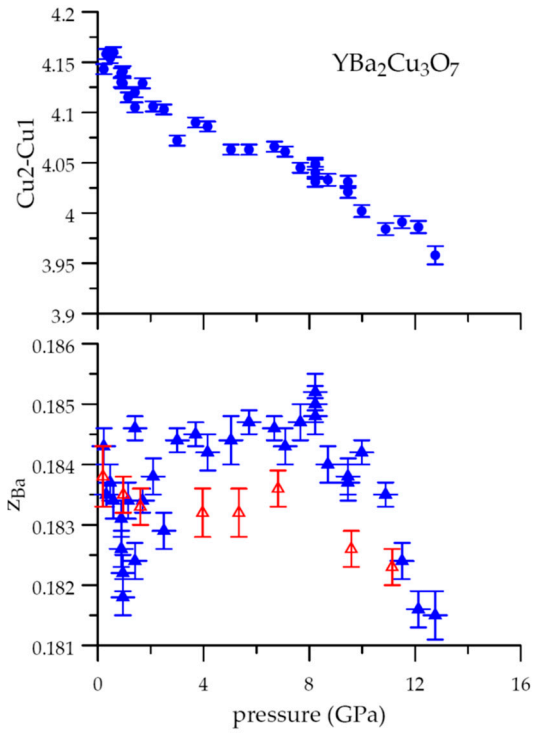

Figure 13. Pressure dependence for Y1237 of Ba atom z-relative position (as compared with the c-axis) and the Cu2-Cu1 distance in Å (open triangles, for decompression).

The new phase and the lattice anomalies could not be related with a non-hydrostatic environment of the transmitting medium. Although the line width of the luminescence line of ruby and the XRD line width cannot provide a definite proof of a hydrostatic medium, no broadening was observed before the 12.7 GPa pressure. Furthermore, the two-dimensional (2D) patterns in the synchrotron detector do not bear any sign of a non-hydrostatic pressure for the lines of the main phase. This is in complete agreement with all measurements performed up to now that do not provide any evidence for a non-hydrostatic environment in the methanol-ethanol mixture for pressures up to 10 GPa [150]. It was also not related to any oxygen deficiency, as the apex mode of the Raman spectra indicate fully oxygenated compounds (Figure 4). In order to investigate the effect of doping and the transmitting medium, the $La_{2-x}Sr_xCuO_4$ system has been examined at hydrostatic pressures by Raman spectroscopy for selected doping levels using the same methanol-ethanol transmitting medium and synchrotron XRD with two different media, i.e., a mixture of methanol-ethanol and neon [151].

Concerning the effect of the transmitting medium, it was found that T_c gradually increases when $Bi_2Sr_2CaCu_2O_8$ is exposed to methanol at room temperature, reaching the maximum T_c after a month [152]. The whole process could be accelerated substantially under hydrostatic pressures. But in the same work no change in T_c was detected for the $La_{2-x}Sr_xCuO_4$ and $YBa_2Cu_3O_7$ compounds. In another systematic investigation of the effect of methanol on $La_{2-x}Sr_xCuO_4$, it was discovered that the adsorption of methanol depends on the amount of Sr via the smaller Cu^{+3} ions in the compound, which facilitate intercalation and the whole effect peaks around x = 0.2 doping [153]. Again, hydrostatic pressure should accelerate and possibly modify the process. Synchrotron XRD data collected on the same La_2CuO_4 compound with a mixture of methanol-ethanol and neon have really detected differences that begin around 7 to 8 GPa [151]. This pressure region almost coincides with the anomalies observed in both Y1237 and Pr1237 (Figure 11), strongly suggesting that the origin of this effect is related to the presence of methanol. For some reason in Y1248 no such effect has been observed (Figure 11)

and this requires further high-pressure investigation using another transmitting medium. In any case, the effect observed both Y1237 and Y1248 at lower pressures (~3 to 4 GPa, Figure 11) must be related to an intrinsic instability of the lattice in these compounds, independent of the transmitting medium.

Concerning the $La_{2-x}Sr_xCuO_4$ compound, synchrotron XRD and Raman data indicate modifications with pressure that depend on the amount of Sr doping [151]. The top section of Figure 14 presents the results for the c-axis of $La_{1.85}Sr_{0.15}CuO_4$ and pure La_2CuO_4 systems. For the x = 0.15 case, the XRD measurements show a deviation around 3 GPa, which disappears for the case of pure La_2CuO_4. As in the cases of yttrium systems, it also shows a hysteresis effect (Figure 14). The bottom portion of Figure 14 presents the pressure dependence of the La/Sr mode for the case of x = 0.15. Something similar, but a smaller effect, happens for the apex phonon [151]. It is clear that Raman data indicate a deviation from linear pressure dependence at ~3 GPa, i.e., the same pressure where the c-axis deviates from normal EOS. Preliminary high-pressure Raman measurements show that the effect depends strongly on the amount of doping [151]. Similar conclusions are obtained from the FWHM of the 004, 103, and 110 diffraction lines [151].

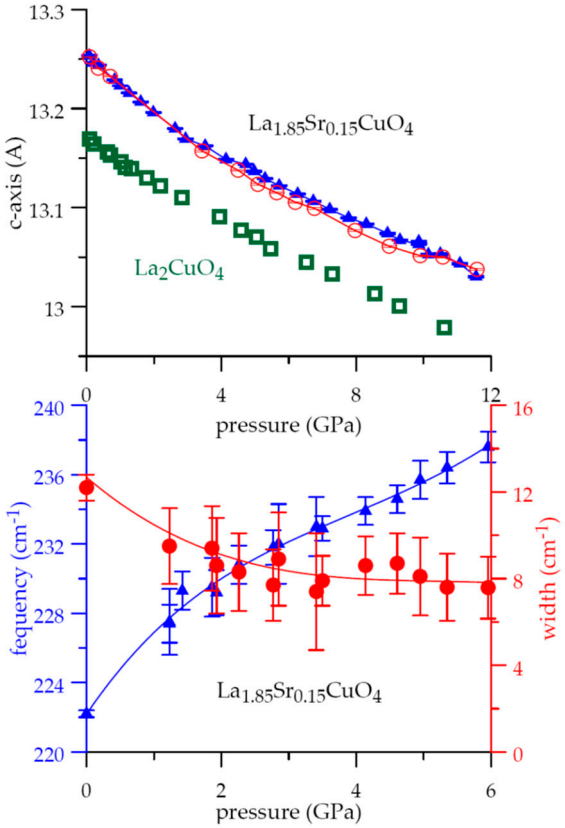

Figure 14. Top: dependence of the c-axis for $La_{1.85}Sr_{0.15}CuO_4$ at increasing (triangles), decreasing (circles) pressures, and for increasing pressure of La_2CuO_4 (squares). **Bottom:** pressure dependence of the La/Sr phonon energy (triangles) and width (circles) of $La_{1.85}Sr_{0.15}CuO_4$.

The effect originates from an anomalous pressure dependence of the apical oxygen position along the c-axis. The La/Sr-O(2) and Cu-O(2) bond length modifications along the c-axis are indications of charge redistribution with hydrostatic pressure [154]. It is also interesting that the tolerance factor, t, calculated from the average distance of the La-O bond lengths, as compared with those of the Cu-O ones [$t = d_{LaO}/\sqrt{2}d_{CuO}$] and associated with charge redistribution [155], also shows an anomaly at ~2 GPa for the optimally doped compound. Furthermore, the tolerance factor appears to jump among different almost equidistant values discontinuously [151]. Although the statistics is not good enough to verify this effect and draw final conclusions, this could be related to the abrupt changes observed

for the Cu_{pl}-O_{ap} in the system $Y_{1-y}Ca_yBa_2Cu_3O_7$ (Figure 9), and the plateaus observed in the Raman measurements under hydrostatic pressure (Figure 12). Such effects could be described as a signature of a stepwise modification of the carrier concentration in the superconducting planes, as in topologically distinct states.

3. Conclusions

Raman studies on a series of cuprates were presented showing lattice distortions induced either by chemical doping or by applying hydrostatic pressure. From the spectral modifications (frequency and width) of the apex and in-phase phonons of the yttrium compounds it was found that the oxygen non-stoichiometry is related with the ordering of the chain oxygen atoms creating separation into submicron phases with varying transition temperature. Our Raman and more recent measurements [122–124] prove that these phases coexist in the $YBa_2Cu_3O_x$ compounds and only the relative amount of the phases varies with doping. Just above the optimum doping, another lattice effect was discovered from the softening of the in-phase mode, which is related to a slight reduction of the transition temperature and originates from a sudden change in the CuO_2 buckling, as verified by other techniques [125,126].

From the study of the Raman active B_{1g} mode it was found that rare earth substitution for yttrium in the same series of superconductors induces a separation into superconducting and non-superconducting phases. Depending on the relative size and the kind of the substituting rare earth element this affects the ability of the compound to superconduct and the transition temperature. Overdoping by Ca substitution for Y shows a very similar phase separation behavior.

Hydrostatic pressure was found to create small lattice distortions in $YBa_2Cu_3O_7$ and $YBa_2Cu_4O_8$ compounds, which are absent for the non-superconducting $PrBa_2Cu_3O_7$ system. The same happens for the $La_{2-x}Sr_xCuO_4$ series, which again disappear in the pure non-superconducting La_2CuO_4 system. Raman studies under hydrostatic pressure in the Bi-cuprates [141] also indicate pressure-induced lattice anomalies at low hydrostatic pressures. In all cases, there are indications for charge redistribution, which apparently affects the carrier concentration in the superconducting planes and modifies T_c.

Raman studies on other high T_c compounds, such as the diborides [60,62,63,102] and the pnictides [103–105], have revealed phase separation and local lattice distortions. This is an indication that the observed effects possibly characterize most of the high temperature superconductors. In all cases, (cuprates, pnictides, and diborides) the lattice anomalies are accompanied by modifications in the transition temperature, indicating some connection between the two effects. It is unclear whether the observed effects are related to the pairing mechanism, although the lattice modifications or the phase separation phenomena apparently induce charge redistribution between the superconducting and the insulating planes in the studied layered structured superconductors. They certainly show that the lattice degrees of freedom participate in the related phenomena to an extent that needs to be clarified.

Funding: This research received no external funding.

Conflicts of Interest: The author declares no conflict of interest.

References

1. Yukalov, V.I. Heterophase fluctuations in ferroelectrics. *Ferroelectrics* **1988**, *82*, 11–24. [CrossRef]
2. Yukalov, V.I. Phase transitions and heterophase fluctuations. *Phys. Rep.* **1991**, *208*, 395–489. [CrossRef]
3. Nagaev, E.L. Phase-separation mechanism for giant magnetoresistance of lanthanum manganites. *Phys. Lett. A* **1996**, *218*, 367–372. [CrossRef]
4. Lanzara, A.; Saini, N.L.; Brunelli, M.; Natali, F.; Bianconi, A.; Radaelli, P.G.; Cheong, S.W. Crossover from large to small polarons across the metal-insulator transition in manganites. *Phys. Rev. Lett.* **1998**, *81*, 878–881. [CrossRef]

5. Yunoki, S.; Hu, J.; Malvezzi, A.L.; Moreo, A.; Furukawa, N.; Dagotto, E. Phase separation in electronic models for manganites. *Phys. Rev. Lett.* **1998**, *80*, 845–848. [CrossRef]
6. Uehara, M.; Mori, S.; Chen, C.H.; Cheong, S.W. Percolative phase separation underlies colossal magnetoresistance in mixed-valent manganites. *Nature* **1999**, *399*, 560–563. [CrossRef]
7. Kagan, M.Y.; Kugel, K.I. Inhomogeneous charge distributions and phase separation in manganites. *Phys. Uspekhi* **2001**, *44*, 553–570. [CrossRef]
8. Kagan, M.Y.; Klaptsov, A.V.; Brodsky, I.V.; Kugel, K.I.; Sboychakov, A.O.; Rakhmanov, A.L. Nanoscale phase separation in manganites. *J. Phys. A Math. Gen.* **2003**, *36*, 9155–9164. [CrossRef]
9. Dagotto, E.; Burgy, J.; Moreo, A. Nanoscale phase separation in colossal magnetoresistance materials: Lessons for the cuprates? *Solid State Commum.* **2003**, *126*, 9–22. [CrossRef]
10. Dagotto, E. Complexity in strongly correlated electronic systems. *Science* **2005**, *309*, 257–262. [CrossRef]
11. Tokura, Y. Critical features of colossal magnetoresistive manganites. *Rep. Prog. Phys.* **2006**, *69*, 797–851. [CrossRef]
12. Hayden, S.M.; Lander, G.H.; Zaretsky, J.; Brown, P.J.; Stassis, C.; Metcalf, P.; Honig, J.M. Incommensurate magnetic correlations in $La_{1.8}Sr_{0.2}NiO_4$. *Phys. Rev. Lett.* **1992**, *68*, 1061. [CrossRef] [PubMed]
13. Campi, G.; Poccia, N.; Joseph, B.; Bianconi, A.; Mishra, S.; Lee, J.; Roy, S.; Nugroho, A.A.; Buchholz, M.; Braden, M.; et al. Direct Visualization of Spatial Inhomogeneity of Spin Stripes Order in $La_{1.72}Sr_{0.28}NiO_4$. *Condens. Matter* **2019**, *4*, 77. [CrossRef]
14. Testardi, L.R. Structural instability and superconductivity in A-15 compounds. *Rev. Mod. Phys.* **1975**, *47*, 637–648. [CrossRef]
15. Bednorz, J.G.; Müller, K.A. Possible high Tc superconductivity in the Ba-La-Cu-O system. *Z. Phys. B Condens. Matter* **1986**, *64*, 189–193. [CrossRef]
16. Jorgensen, A.J.; Dabrowski, B.; Pei, S.; Hinks, D.G.; Soderholm, L.; Morosin, B.; Schirber, E.L.; Venturini, E.L.; Ginley, D.S. Superconducting phase of $La_2CuO_{4+\delta}$: A superconducting composition resulting from phase separation. *Phys. Rev. B* **1988**, *38*, 11337–11345. [CrossRef]
17. Benedek, G.; Müller, K.A. *Phase Separation in Cuprate Superconductors*; World Scientific: Singapore, 1992.
18. Bianconi, A. *Phase Separation in Cuprate Superconductors*; Müller, K.A., Benedek, G., Eds.; World Scientific: Singapore, 1993; pp. 125–138.
19. Kremer, R.K.; Sigmund, E.; Hizhnyakov, V.; Hentsch, F.; Simon, A.; Müller, K.A.; Mehring, M. Percolative phase separation in $La_2CuO_{4+\delta}$ and $La_{2-x}Sr_xCuO_4$. *Z. Phys. B Condens. Matter* **1992**, *86*, 319–324. [CrossRef]
20. Benedek, G.; Müller, K.A. *Phase Separation in Cuprate Superconductors*; Springer: Berlin/Herdelberg, Germany, 1994.
21. Bianconi, A.; Missori, M. The Coupling of a Wigner Polaronic Charge Density Wave with a Fermi Liquid Arising from the Instability of a Wigner Polaron Crystal: A Possible Pairing Mechanism in High Tc Superconductors. In *Phase Separation in Cuprate Superconductors*; Springer: Berlin/Heidelberg, Germany, 1994; pp. 272–289.
22. Bianconi, A. On the Fermi liquid coupled with a generalized Wigner polaronic CDW giving high Tc superconductivity. *Solid State Commun.* **1994**, *91*, 1–5. [CrossRef]
23. Bianconi, A.; Missori, M. High Tc superconductivity by quantum confinement. *J. Phys.* **1994**, *4*, 361–365.
24. Bianconi, A. On the possibility of new high Tc superconductors by producing metal heterostructures as in the cuprate perovskites. *Solid State Commum.* **1994**, *89*, 933–936. [CrossRef]
25. Hizhnyakov, V.; Sigmund, E.; Seibold, G. Polaron formation and percolative phase separation in HTSC. In *Phase Separation in Cuprate Superconductors*; Springer: Berlin/Heidelberg, Germany, 1994; pp. 50–65.
26. Bianconi, A.; Missori, M.; Oyanagi, H.; Yamaguchi, H.; Ha, D.H.; Nishiara, Y.; Della Longa, S. The measurement of the polaron size in the metallic phase of cuprate superconductors. *Eur. Lett.* **1995**, *31*, 411. [CrossRef]
27. Nagaev, E.L. Phase separation in high-temperature superconductors and related magnetic materials. *Uspekhi Fizicheskikh Nauk* **1995**, *165*, 529–555. [CrossRef]
28. Zech, D.; Conder, K.; Keller, H.; Kaldis, E.; Liarokapis, E.; Poulakis, N.; Müller, K.A. *Anharmonic Properties of High-T_c Cuprates*; Mihailovic, D., Ruani, G., Kaldis, E., Müller, K.A., Eds.; World Scientific: Singapore, 1995; pp. 18–29.
29. Kusmartsev, F.V.; Di Castro, D.; Bianconi, G.; Bianconi, A. Transformation of strings into an inhomogeneous phase of stripes and itinerant carriers. *Phys. Lett. A* **2000**, *275*, 118–123. [CrossRef]

30. Gor'kov, L.P. Phase separation in a two-component model for cuprates. *J. Supercond.* **2000**, *13*, 765–769. [CrossRef]
31. Bianconi, A.; Di Castro, D.; Bianconi, G.; Pifferi, A.; Saini, N.L.; Chou, F.C.; Johnston, D.C.; Colapietro, M. Coexistence of stripes and superconductivity: Tc amplification in a superlattice of superconducting stripes. *Phys. C* **2000**, *341*, 1719–1722. [CrossRef]
32. Coleman, A.J. *Phase Transitions and Self-Organization in Electronic and Molecular Networks*; Phillips, J.C., Thorpe, M.F., Eds.; Kluwer: New York, NY, USA, 2001; pp. 23–35.
33. Phillips, J.C. Percolative model of nanoscale phase separation in high-temperature superconductors. *Philos. Mag. B* **2002**, *82*, 783–790. [CrossRef]
34. Bishop, A.R.; Lookman, T.; Saxena, A.; Shenoy, S.R. Elasticity-driven nanoscale texturing in complex electronic materials. *Eur. Phys. Lett.* **2003**, *63*, 289–295. [CrossRef]
35. Phillips, J.C.; Saxena, A.; Bishop, A.R. Pseudogaps, dopants, and strong disorder in cuprate high-temperature superconductors. *Rep. Prog. Phys.* **2003**, *66*, 2111–2182. [CrossRef]
36. De Mello, E.V.L.; Caixeiro, E.S. Effects of phase separation in the cuprate superconductors. *Phys. Rev. B* **2004**, *70*, 224517. [CrossRef]
37. Kugel, K.I.; Rakhmanov, A.L.; Sboychakov, A.O. Phase separation in Jahn-Teller systems with localized and itinerant electrons. *Phys. Rev. Lett.* **2005**, *95*, 267210. [CrossRef]
38. De Mello, E.V.L.; Dias, D.H.N. Phase separation and the phase diagram of cuprate superconductors. *J. Phys. Condens. Matter* **2007**, *19*, 086218. [CrossRef]
39. Fine, B.V.; Egami, T. Phase separation in the vicinity of quantum-critical doping concentration: Implications for high-temperature superconductors. *Phys. Rev. B* **2008**, *77*, 014519. [CrossRef]
40. Kugel, K.I.; Rakhmanov, A.L.; Sboychakov, A.O.; Poccia, N.; Bianconi, A. Model for phase separation controlled by doping and the internal chemical pressure in different cuprate superconductors. *Phys. Rev. B* **2008**, *78*, 165124. [CrossRef]
41. Fratini, M.; Poccia, N.; Bianconi, A. The Feshbach resonance and nanoscale phase separation in a polaron liquid near the quantum critical point for a polaron Wigner crystal. *J. Phys.* **2008**, *108*, 012036. [CrossRef]
42. Innocenti, D.; Ricci, A.; Poccia, N.; Campi, G.; Fratini, M.; Bianconi, A. A model for liquid-striped liquid phase separation in liquids of anisotropic polarons. *J. Supercond. Nov. Magn.* **2009**, *22*, 529–533. [CrossRef]
43. De Mello, E.V.L.; Kasal, R.B.; Passos, C.A.C. Electronic phase separation transition as the origin of the superconductivity and pseudogap phase of cuprates. *J. Phys. Condens. Matter* **2009**, *21*, 235701. [CrossRef]
44. Fratini, M.; Poccia, N.; Ricci, A.; Campi, G.; Burghammer, M.; Aeppli, G.; Bianconi, A. Scale-free structural organization of oxygen interstitials in La_2CuO_{4+y}. *Nature* **2010**, *466*, 841–844. [CrossRef]
45. Poccia, N.; Fratini, M.; Ricci, A.; Campi, G.; Barba, L.; Vittorini-Orgeas, A.; Bianconi, G.; Aeppli, G.; Bianconi, A. Evolution and control of oxygen order in a cuprate superconductor. *Nat. Mater.* **2011**, *10*, 733–736. [CrossRef]
46. Poccia, N.; Ricci, A.; Campi, G.; Fratini, M.; Puri, A.; Di Gioacchino, D.; Marcelli, A.; Reynolds, M.; Burghammer, M.; Saini, N.L.; et al. Optimum inhomogeneity of local lattice distortions in La_2CuO_{4+y}. *Proc. Natl. Acad. Sic. USA* **2012**, *109*, 15685–15690. [CrossRef]
47. Pinheiro, C.F.S.; De Mello, E.V.L. Random resistivity network calculations for cuprate superconductors with an electronic phase separation transition. *Physica A* **2012**, *391*, 1532–1539. [CrossRef]
48. De Mello, E.V.L. Describing how the superconducting transition in La_2CuO_{4+y} is related to the iO phase separation. *J. Supercond. Nov. Magn.* **2012**, *25*, 1347–1350. [CrossRef]
49. De Mello, E.V.L. Description and connection between the oxygen order evolution and the superconducting transition in La_2CuO_{4+y}. *Eur. Phys. Lett.* **2012**, *98*, 57008. [CrossRef]
50. Phillips, J.C. Ineluctable complexity of high temperature superconductivity elucidated. *J. Supercond. Nov. Magn.* **2014**, *27*, 345–347. [CrossRef]
51. Bianconi, A.; Poccia, N.; Sboychakov, A.O.; Rakhmanov, A.L.; Kugel, K.I. Intrinsic arrested nanoscale phase separation near a topological Lifshitz transition in strongly correlated two-band metals. *Supercond. Sci. Technol.* **2015**, *28*, 024005. [CrossRef]
52. Campi, G.; Bianconi, A.; Poccia, N.; Bianconi, G.; Barba, L.; Arrighetti, G.; Innocenti, D.; Karpinski, J.; Zhigadlo, N.D.; Kazakov, S.M.; et al. Inhomogeneity of charge-density-wave order and quenched disorder in a high-Tc superconductor. *Nature* **2015**, *525*, 359–362. [CrossRef]

53. Agrestini, S.; Saini, N.L.; Bianconi, G.; Bianconi, A. The strain of CuO_2 lattice: The second variable for the phase diagram of cuprate perovskites. *J. Phys. A Math. Gen.* **2003**, *36*, 9133–9142. [CrossRef]
54. Campi, G.; Ricci, A.; Poccia, N.; Fratini, M.; Bianconi, A. X-rays Writing/Reading of charge density waves in the CuO_2 plane of a simple cuprate superconductor. *Condens. Matter* **2017**, *2*, 26. [CrossRef]
55. Campi, G.; Bianconi, A. Evolution of complexity in out-of-equilibrium systems by time-resolved or space-resolved synchrotron radiation techniques. *Condens. Matter* **2019**, *4*, 32. [CrossRef]
56. Phillips, J.C. *Physics of High-Tc Superconductors*; Academic: Boston, MA, USA, 1989.
57. Nagamatsu, J.; Nakagawa, N.; Muranaka, T.; Zenitani, Y.; Akimitsu, J. Superconductivity at 39 K in magnesium diboride. *Nature* **2001**, *410*, 63–64. [CrossRef]
58. Bauer, E.; Paul, C.; Berger, S.; Majumdar, S.; Michor, H.; Giovannini, M.; Saccone, A.; Bianconi, A. Thermal conductivity of superconducting MgB_2. *J. Phys. Condens. Mat.* **2001**, *13*, L487–L493. [CrossRef]
59. Agrestini, S.; Di Castro, D.; Sansone, M.; Saini, N.L.; Saccone, A.; De Negri, S.; Giovannini, M.; Colapietro, M.; Bianconi, A. High Tc superconductivity in a critical range of micro-strain and charge density in diborides. *J. Phys. Condens. Matter* **2001**, *13*, 11689–11695. [CrossRef]
60. Agrestini, S.; Metallo, C.; Filippi, M.; Simineli, L.; Campi, G.; Sanipoli, C.; Liarokapis, E.; De Negri, S.; Giovannini, M.; Saccone, A.; et al. Substitution of Sc for Mg in MgB_2: Effects on transition temperature and Kohn anomaly. *Phys. Rev. B* **2004**, *70*, 134514. [CrossRef]
61. Palmisano, V.; Simonelli, L.; Puri, A.; Fratini, M.; Busby, Y.; Parisiades, P.; Liarokapis, E.; Brunelli, M.; Fitch, A.N.; Bianconi, A. Controlling mesoscopic phase separation near electronic topological transitions via quenched disorder in ternary diborides. *J. Phys. Condens. Matter* **2008**, *20*, 434222. [CrossRef]
62. Simonelli, L.; Palmisano, V.; Fratini, M.; Paridiades, P.; Lampakis, D.; Liarokapis, E.; Bianconi, A. Isotope effect on the E_{2g} phonon and mesoscopic phase separation near the electronic topological transition in $Mg_{1-x}Al_xB_2$. *Phys. Rev. B* **2009**, *80*, 014520. [CrossRef]
63. Parisiades, P.; Liarokapis, E. Lattice effects in diborides. *J. Supercond. Nov. Magn.* **2011**, *24*, 49–56. [CrossRef]
64. Hebard, A.F.; Rosseinsky, M.J.; Haddon, R.C.; Murphy, D.W.; Glarum, S.H.; Palstra, T.T.M.; Ramirez, A.P.; Kortan, A.R. Superconductivity at 18 K in potassium doped C60. *Nature* **1991**, *350*, 600–601. [CrossRef]
65. Zhou, O.; Zhu, Q.; Fischer, J.E.; Coustel, N.; Vaughan, G.B.M.; Heiney, P.A.; McCauley, J.P., Jr.; Smith, A.B. Compressibility of M3C60 fullerene superconductors: Relation between Tc and lattice parameter. *Science* **1992**, *255*, 833–835. [CrossRef]
66. Palstra, T.T.M.; Zhou, O.; Iwasa, Y.; Sulewski, P.E.; Fleming, R.M.; Zegarski, B.R. Superconductivity at 40K in cesium doped C60. *Solid State Commum.* **1995**, *93*, 327–330. [CrossRef]
67. Drozdov, A.P.; Eremets, M.I.; Troyan, I.A.; Ksenofontov, V.; Shylin, S.I. Conventional superconductivity at 203 kelvin at high pressures in the sulfur hydride system. *Nature* **2015**, *525*, 73–76. [CrossRef]
68. Bianconi, A.; Jarlborg, T. Superconductivity above the lowest Earth temperature in pressurized sulfur hydride. *Eur. Phys. Lett.* **2015**, *112*, 37001. [CrossRef]
69. Jarlborg, T.; Bianconi, A. Breakdown of the Migdal approximation at Lifshitz transitions with giant zero-point motion in the H3S superconductor. *Sci. Rep.* **2016**, *6*, 24816. [CrossRef]
70. Bianco, R.; Errea, I.; Calandra, M.; Mauri, F. High-pressure phase diagram of hydrogen and deuterium sulfides from first principles: Structural and vibrational properties including quantum and anharmonic effects. *Phys. Rev. B* **2018**, *97*, 214101. [CrossRef]
71. Bianconi, A.; Saini, N.L.; Lanzara, A.; Missori, M.; Rossetti, T.; Oyanagi, H.; Yamaguchi, H.; Oka, K.; Ito, T. Determination of the lattice Distortions in the CuO_2 Plane of $La_{1.85}Sr_{0.15}CuO_4$. *Phys. Rev. Lett.* **1996**, *76*, 3412–3415. [CrossRef] [PubMed]
72. Lanzara, A.; Zhao, G.M.; Saini, N.L.; Bianconi, A.; Conder, K.; Keller, H.; Müller, K.A. Oxygen-isotope shift of the charge-stripe ordering temperature in $La_{2-x}Sr_xCuO_4$ from x-ray absorption spectroscopy. *J. Phys. Condens. Matter* **1999**, *11*, L541–L546. [CrossRef]
73. Lanzara, A.; Bogdanov, P.V.; Zhou, X.J.; Kellar, S.A.; Feng, D.L.; Lu, E.D.; Yoshida, T.; Eisaki, H.; Fujimori, A.; Kishio, K.; et al. Evidence for ubiquitous strong electron-phonon coupling in high-temperature superconductors. *Nature* **2001**, *412*, 510–514. [CrossRef] [PubMed]
74. Shen, Z.X.; Lanzara, A.; Ishihara, S.; Nagaosa, N. Role of the electron-phonon interaction in the strongly correlated cuprate superconductors. *Philos. Mag. B* **2002**, *82*, 1349–1368. [CrossRef]
75. Gweon, G.H.; Sasagawa, T.; Zhou, S.Y.; Graf, J.; Takagi, H.; Lee, D.H.; Lanzara, A. An unusual isotope effect in a high-transition-temperature superconductor. *Nature* **2004**, *430*, 187–190. [CrossRef]

76. Graf, J.; Jozwiak, C.; Smallwood, C.L.; Eisaki, H.; Kaindl, R.A.; Lee, D.H.; Lanzara, A. Nodal quasiparticle meltdown in ultrahigh-resolution pump-probe angle-resolved photoemission. *Nat. Phys.* **2011**, *7*, 805–809. [CrossRef]
77. Perali, A.; Innocenti, D.; Valletta, A.; Bianconi, A. Anomalous isotope effect near a 2.5 Lifshitz transition in a multi-band multi-condensate superconductor made of a superlattice of stripes. *Supercond. Sci. Technol.* **2012**, *25*, 124002. [CrossRef]
78. Guguchia, Z.; Khasanov, R.; Bendele, M.; Pomjakushina, E.; Conder, K.; Shengelaya, A.; Keller, H. Negative Oxygen Isotope Effect on the Static Spin Stripe Order in Superconducting $La_{2-x}Ba_xCuO_4$ (x = 1/8) Observed by Muon-Spin Rotation. *Phys. Rev. Lett.* **2014**, *113*, 057002. [CrossRef]
79. Bendele, M.; von Rohr, F.; Guguchia, Z.; Pomjakushina, E.; Conder, K.; Bianconi, A.; Simon, A.; Bussmann-Holder, A.; Keller, H. Evidence for strong lattice effects as revealed from huge unconventional oxygen isotope effects on the pseudogap temperature in $La_{2-x}Sr_xCuO_4$. *Phys. Rev. B* **2017**, *95*, 014514. [CrossRef]
80. Caivano, R.; Fratini, M.; Poccia, N.; Ricci, A.; Puri, A.; Ren, Z.A.; Dong, X.L.; Yang, J.; Lu, W.; Zhao, Z.X.; et al. Feshbach resonance and mesoscopic phase separation near a quantum critical point in multiband FeAs-based superconductors. *Supercond. Sci. Technol.* **2008**, *22*, 014004. [CrossRef]
81. Ricci, A.; Poccia, N.; Campi, G.; Joseph, B.; Arrighetti, G.; Barba, L.; Reynolds, M.; Burghammer, M.; Takeya, H.; Mizuguchi, Y.; et al. Nanoscale phase separation in the iron chalcogenide superconductor $K_{0.8}Fe_{1.6}Se_2$ as seen via scanning nanofocused x-ray diffraction. *Phys. Rev. B* **2011**, *84*, 060511. [CrossRef]
82. Bianconi, A. Quantum materials: Shape resonances in superstripes. *Nat. Phys.* **2013**, *9*, 536–537. [CrossRef]
83. Bendele, M.; Barinov, A.; Joseph, B.; Innocenti, D.; Iadecola, A.; Bianconi, A.; Takeya, H.; Mizuguchi, Y.; Takano, T.; Noji, T.; et al. Spectromicroscopy of electronic phase separation in $K_xFe_{2-y}Se_2$ superconductor. *Sci. Rep.* **2014**, *4*, 5592. [CrossRef]
84. Ricci, A.; Poccia, N.; Joseph, B.; Innocenti, D.; Campi, G.; Zozulya, A.; Westermeier, A.; Schavkan, A.; Coneri, F.; Bianconi, A.; et al. Direct observation of nanoscale interface phase in the superconducting chalcogenide $K_xFe_{2-y}Se_2$ with intrinsic phase separation. *Phys. Rev. B* **2015**, *91*, 020503. [CrossRef]
85. Simonelli, L.; Mizokawa, T.; Sala, M.M.; Takeya, H.; Mizuguchi, Y.; Takano, Y.; Garbarino, G.; Monaco, G.; Saini, N.L. Temperature dependence of iron local magnetic moment in phase-separated superconducting chalcogenide. *Phys. Rev. B* **2014**, *90*, 214516. [CrossRef]
86. Mangelis, P.; Lei, H.; McDonnell, M.; Feygenson, M.; Petrovic, C.; Bozin, E.; Lappas, A. On the Nanoscale Structure of $K_xFe_{2-y}Ch_2$ (Ch=S, Se): A Neutron Pair Distribution Function View. *Condens. Matter* **2018**, *3*, 20. [CrossRef]
87. Bianconi, A. Multiplet splitting of final-state configurations in x-ray-absorption spectrum of metal VO_2: Effect of core-hole-screening, electron correlation, and metal-insulator transition. *Phys. Rev. B* **1982**, *26*, 2741. [CrossRef]
88. Marcelli, A.; Coreno, M.; Stredansky, M.; Xu, W.; Zou, C.; Fan, L.; Wangsheng, C.; Wei, S.; Cossaro, A.; Ricci, A.; et al. Nanoscale phase separation and lattice complexity in VO2: The metal-insulator transition investigated by XANES via Auger electron yield at the vanadium L_{23}-edge and resonant photoemission. *Condens. Matter* **2017**, *2*, 38. [CrossRef]
89. Gioacchino, D.; Marcelli, A.; Puri, A.; Zou, C.; Fan, L.; Zeitler, U.; Bianconi, A. Metastability phenomena in VO2 thin films. *Condens. Matter* **2017**, *2*, 10. [CrossRef]
90. Corder, S.N.G.; Jiang, J.; Chen, X.; Kittiwatanakul, S.; Tung, I.C.; Zhu, Y.; Zhang, J.; Bechtel, H.; Martin, M.C.; Carr, L.G.; et al. Controlling phase separation in vanadium dioxide thin films via substrate engineering. *Phys. Rev. B* **2017**, *96*, 161110. [CrossRef]
91. Vidas, L.; Günther, C.M.; Miller, T.A.; Pfau, B.; Perez-Salinas, D.; Martínez, E.; Schneider, M.; Guhrs, E.; Gargiani, P.; Valvidares, M.; et al. Imaging Nanometer Phase Coexistence at Defects During the Insulator-Metal Phase Transformation in VO_2 Thin Films by Resonant Soft X-ray Holography. *Nano Lett.* **2018**, *18*, 3449–3453. [CrossRef] [PubMed]
92. Grandi, F.; Amaricci, A.; Fabrizio, M. Unraveling the Mott-Peierls intrigue in Vanadium dioxide. *arXiv* **2019**, arXiv:1906.10632.
93. Thomsen, C. *Light Scattering in Solids*; Cardona, M., Guntherodt, G., Eds.; Springer-Verlag: Berlin, Germany, 1991; Volume VI, pp. 285–359.

94. Iliev, M.N.; Thomsen, C.; Hadjiev, V.; Cardona, M. Resonant Raman scattering of oxygen-deficient $YBa_2Cu_3O_{7-\delta}$: Evidence for the coexistence of ortho-I, ortho-II, and tetragonal microstructures. *Phys. Rev. B* **1993**, *47*, 12341–12344. [CrossRef]
95. Poulakis, N.; Palles, D.; Liarokapis, E.; Conder, K.; Kaldis, E.; Müller, K.A. Phase separation and softening of the O2,3 in-phase mode in the $YBa_2Cu_3O_x$ superconductors. *Phys. Rev. B* **1996**, *53*, 219–220. [CrossRef]
96. Mihailovic, D.; McCarty, K.F.; Ginley, D.S. Anharmonic properties and the two-particle continuum in the Raman spectra of $YBa_2Cu_3O_{6.9}$, $TlBa_2CaCu_2O_7$, and $Tl_2Ba_2CaCu_2O_8$. *Phys. Rev. B* **1993**, *47*, 8910–8916. [CrossRef]
97. Ruani, G.; Taliani, C.; Muccini, M.; Conder, K.; Kaldis, M.; Keller, H.; Zech, D.; Muller, K.A. Apex anharmonicity observed by Raman scattering in ^{18}O substituted $YBa_2Cu_3O_{6+x}$. *Physica C* **1994**, *226*, 101–105. [CrossRef]
98. Palles, D.; Poulakis, N.; Liarokapis, E.; Conder, K.; Kaldis, E.; Muller, K.A. Raman study of the oxygen anharmonicity in $YBa_2Cu_3O_x$ ($6.4 < x < 7.0$) superconductors. *Phys. Rev. B* **1996**, *54*, 6721–6727.
99. Cooper, S.L.; Slakey, F.; Klein, M.V.; Rice, J.P.; Bukowski, E.D.; Ginsberg, D.M. Gap anisotropy and phonon self-energy effects in single-crystal $YBa_2Cu_3O_{7-\delta}$. *Phys. Rev. B* **1988**, *38*, 11934–11937. [CrossRef]
100. Deveraux, T.P.; Einzel, D.; Stadlober, B.; Hackl, R.; Leach, D.H.; Neumeier, J.J. Electronic Raman scattering in high-T_c superconductors: A probe of d_{x2-y2} pairing. *Phys. Rev. Lett.* **1994**, *72*, 396–399. [CrossRef] [PubMed]
101. Heyen, E.T.; Wegerer, R.; Schonherr, E.; Cardona, M. Raman study of the coupling of crystal-field excitations to phonons in $NdBa_2Cu_3O_{7-\delta}$. *Phys. Rev. B* **1991**, *44*, 10195–10205. [CrossRef] [PubMed]
102. Parisiades, P.; Lampakis, D.; Palles, D.; Liarokapis, E.; Zhigadlo, N.D.; Katrysh, S.; Karpinski, J. Two-mode behavior for the E_{2g} broad band in $Mg(B_{1-x}C_x)_2$. *Phys. C* **2008**, *468*, 1064–1069. [CrossRef]
103. Calamiotou, M.; Margiolaki, I.; Gantis, A.; Siranidi, E.; Ren, Z.A.; Zhao, Z.X.; Liarokapis, E. Lattice anomalies in the $FeAs_4$ tetrahedra of the $NdFeAsO_{0.85}$ superconductor that disappear at T_c. *Eur. Phys. Lett.* **2010**, *91*, 57005. [CrossRef]
104. Liarokapis, E.; Calamiotou, M.; Zhigadlo, N.D.; Katrysh, S.; Karpinski, J. Non-linera lattice response of Sm oxypnictides to hydrostatic pressure. *J. Phys. Chem. Solid* **2013**, *74*, 1465–1469. [CrossRef]
105. Calamiotou, M.; Lampakis, D.; Zhigadlo, N.D.; Katrysh, S.; Karpinski, J.; Fitch, A.; Tsiaklaganos, P.; Liarokapis, E. Local lattice distortions vs. structural phase transition in $NdFeAsO_{1-x}F_x$. *Phys. C* **2016**, *527*, 55–62. [CrossRef]
106. Thomsen, C.; Cardona, M. *Physical Properties of High Temperature Superconductors*; Ginsberg, D.M., Ed.; World Scientific: Singapore, 1994; p. 409.
107. Plakida, N.M. *High Temperature Superconductivity*; Springer-Verlag: Berlin, Germany, 1995.
108. FacFarlane, R.M.; Rosen, H.J.; Engler, E.M.; Jacowitz, R.D.; Lee, V.Y. Raman study of the effect of oxygen stoichiometry on the phonon spectrum of the high-T_c superconductor $YBa_2Cu_3O_x$. *Phys. Rev. B* **1988**, *38*, 284–289. [CrossRef]
109. Wille, L.T.; Berera, A.; deFontaine, D. Thermodynamics of oxygen ordering in $YBa_2Cu_3O_z$. *Phys. Rev. Lett.* **1988**, *60*, 1065–1068. [CrossRef]
110. Cava, R.J.; Hewat, A.W.; Hewat, E.A.; Batlogg, B.; Marezio, M.; Rabe, K.M.; Krajewski, J.J.; Peck, W.F.; Rupp, L.W., Jr. Structural anomalies, oxygen ordering and superconductivity in oxygen deficient $Ba_2YCu_3O_x$. *Physica C* **1990**, *165*, 419–433. [CrossRef]
111. Schleger, P.; Casalta, H.; Hadfield, R.; Poulsen, H.F.; von Zimmermann, M.; Andersen, N.H.; Schneider, J.R.; Liang, R.; Dosanjh, P.; Hardy, W.N. Observation of ortho-III correlations by neutron and hard X-ray scattering in an untwined $YBa_2Cu_3O_{6.77}$ single crystal. *Physica C* **1995**, *241*, 103–110. [CrossRef]
112. Dagotto, E. Correlated electrons in high-temperature superconductors. *Rev. Mod. Phys.* **1992**, *66*, 763–841. [CrossRef]
113. Heyen, E.T.; Kircher, J.; Cardona, M. Resonant Raman scattering in insulating $YBa_2Cu_3O_6$ as a probe of its electronic structure. *Phys. Rev. B* **1992**, *45*, 3037–3047, and references therein. [CrossRef] [PubMed]
114. Denisov, V.N.; Taliani, C.; Mal'shukov, A.G.; Burlakov, V.M.; Schonherr, E.; Ruani, G. Infrared excited Raman scattering and photoluminescence of deep intragap states in semiconducting $YBa_2Cu_3O_{6+x}$. *Phys. Rev. B* **1993**, *48*, 16714–16721. [CrossRef] [PubMed]
115. Mesot, J.; Allenspach, P.; Staub, U.; Furrer, A.; Mutka, H. Neutron spectroscopic evidence for cluster formation and percolative superconductivity in $ErBa_2Cu_3O_x$. *Phys. Rev. Lett.* **1993**, *70*, 865–868. [CrossRef]

116. Liarokapis, E. Raman spectroscopy, structural modifications and phase transitions in the high-temperature superconductors. *J. Supercond.* **2000**, *13*, 889–893. [CrossRef]
117. Pintschovius, L.; Reichardt, W. Inelastic neutron scattering studies of the lattice vibrations of high T_c compounds. In *Physical Properties of High Temperature Superconductors*; Ginsberg, D.M., Ed.; World Scientific: Singapore, 1994; pp. 295–374.
118. Reyes-Gasga, J.; Krekels, T.; van Tendeloo, G.; van Landuyt, J.; Amelinckx, S.; Bruggink, W.H.M.; Verweij, H. 3-d vacancy ordered superstructures in "homogeneous" $YBa_2Cu_3O_{7-\delta}$. *Physica C* **1989**, *159*, 831–848. [CrossRef]
119. Alario-Franco, M.A.; Chaillout, C.; Capponi, J.J.; Chenavas, J.; Marezio, M. A family of non-stoichiometric phases based on $Ba_2YCu_3O_{7-\delta}$ ($0 \leq \delta \leq 1$). *Physica C* **1988**, *156*, 455–460. [CrossRef]
120. Sonntag, R.; Hohlwein, D.; Brückel, T.; Collin, G. First observation of superstructure reflections by neutron diffraction due to oxygen ordering in $YBa_2Cu_3O_{6.35}$. *Phys. Rev. Lett.* **1991**, *66*, 1497–1500. [CrossRef]
121. Zimmermann, V.M.; Schneider, J.R.; Frello, T.; Andersen, N.H.; Madsen, J.; Käll, M.; Poulsen, H.F.; Liang, R.; Dosanjh, P.; Hardy, W.N. Oxygen-ordering superstructures in underdoped $YBa_2Cu_3O_{6+x}$ studied by hard x-ray diffraction. *Phys. Rev. B* **2003**, *68*, 104515. [CrossRef]
122. Ricci, A.; Poccia, N.; Campi, G.; Coneri, F.; Caporale, A.S.; Innocenti, D.; Burghammer, M.V.; Zimmermann, M.; Bianconi, A. Multiscale distribution of oxygen puddles in 1/8 doped $YBa_2Cu_3O_{6.67}$. *Sci. Rep.* **2013**, *3*, 2383. [CrossRef]
123. Ricci, A.; Poccia, N.; Campi, G.; Coneri, F.; Barba, L.; Arrighetti, G.; Polentarutti, M.; Burghammer, M.; Sprung, M.V.; Zimmermann, M.; et al. Networks of superconducting nano-puddles in 1/8 doped $YBa_2Cu_3O_{6.5+y}$ controlled by thermal manipulation. *New J. Phys.* **2014**, *16*, 053030. [CrossRef]
124. Campi, G.; Ricci, A.; Poccia, N.; Bianconi, A. Imaging Spatial Ordering of the Oxygen Chains in $YBa_2Cu_3O_{6+y}$ at the Insulator-to-Metal Transition. *J. Supercond. Nov. Mater.* **2014**, *27*, 987–990. [CrossRef]
125. Rohler, J.; Loeffen, P.W.; Mullender, S.; Conder, K.; Kaldis, E. Local structure studies of the underdoped-overdoped transition in $YBa_2Cu_3O_x$. In *High-Tc Superconductivity 1996: Ten Years after the Discovery*; Kaldis, E., Liarokapis, E., Muller, K.A., Eds.; NATO ASI Series; Kluwer Academic Publ.: Dordrecht, The Netherlands, 1997; pp. 469–502.
126. Conder, K.; Zech, D.; Kruger, C.H.; Kaldis, E.; Keller, H.; Hewat, A.W.; Jilek, E. Indications for a phase separation in $YBa_2Cu_3O_{7-x}$. In *Phase Separation in Cuprate Superconductors*; Sigmund, E., Muller, K.A., Eds.; Springer: Berlin/Herdelberg, Germany, 1994; pp. 210–224.
127. Kaldis, E.; Röhler, J.; Liarokapis, E.; Poulakis, N.; Conder, K.; Loeffen, P.W. A displacive structural transformation in the CuO_2 planes of $YBa_2Cu_3O_x$ at the underdoped-overdoped phase separation line. *Phys. Rev. Lett.* **1997**, *79*, 4894–4897. [CrossRef]
128. Calamiotou, M.; Gantis, A.; Palles, D.; Lampakis, D.; Liarokapis, E.; Koufoudakis, A. Phase separation and internal strains in the mixed $La_{0.5}R_{0.5}Ba_2Cu_3O_y$ compounds (R = rare-earth element). *Phys. Rev. B* **1998**, *58*, 15238–15246. [CrossRef]
129. Bogachev, G.; Abrashev, M.; Iliev, M.N.; Poulakis, N.; Liarokapis, E.; Mitros, C.; Koufoudakis, A.; Psyharis, V. Raman study of $R_{0.5}Pr_{0.5}Ba_2Cu_3O_{7-\delta}$. *Phys. Rev. B* **1994**, *49*, 12151–12158. [CrossRef] [PubMed]
130. Palles, D.; Liarokapis, E.; Leventouri, T.H.; Chakoumakos, B.C. The effect of Ca substitution on the structure and the Raman active phonons in $Y_{1-x}Ca_xBa_2Cu_3O_{7-\delta}$. *J. Phys. Condens. Matter* **1998**, *10*, 2515–2524. [CrossRef]
131. Friedl, B.; Thomsen, C.; Cardona, M. Determination of the superconducting gap in $RBa_2Cu_3O_{7-\delta}$. *Phys. Rev. Lett.* **1990**, *65*, 915–918. [CrossRef]
132. Gantis, A.; Calamiotou, M.; Palles, D.; Lampakis, D.; Liarokapis, E. Phase formation and lattice strain in superconducting compound $Y_{1-x}La_xBa_2Cu_3O_y$ ($0 \leq x \leq 1$). *Phys. Rev. B* **2003**, *68*, 064502. [CrossRef]
133. Calamiotou, M.; Gantis, A.; Margiolaki, I.; Palles, D.; Siranidi, E.; Liarokapis, E. Phase separation, microstructure and superconductivity in the $Y_{1-x}Pr_xBa_2Cu_3O_y$ compounds. *J. Condens. Matter* **2008**, *20*, 395224. [CrossRef]
134. Rosen, H.J.; Macfarlane, R.M.; Engler, E.M.; Lee, V.Y.; Jacowitz, R.D. Systematic Raman study of effects of rare-earth substitution on the lattice modes of high Tc superconductors. *Phys. Rev.* **1988**, *38*, 2460–2465. [CrossRef]
135. Chang, I.F.; Mitra, S.S. Long wavelength optical phonons in mixed crystals. *Adv. Phys.* **1971**, *20*, 359–404. [CrossRef]

136. Röhler, J.; Friedrich, C.; Granzow, T.; Kaldis, E.; Böttger, G. *High Temperature Superconductivity*; AIP Conf. Proc. No. 483; Barnes, S.E., Ed.; AIP: New York, NY, USA, 1999; pp. 320–323.
137. Lampakis, D.; Liarokapis, E.; Karpinski, J.; Panagopoulos, C.; Nishizaki, T. Local lattice distortions and phase separation in cuprates. *J. Supercond.* **2004**, *17*, 121–125. [CrossRef]
138. Liarokapis, E.; Lampakis, D.; Palles, D.; Karpinski, J.; Panagopoulos, C. A Raman view of lattice distortions an charge transfer in cuprates. *J. Phys. Chem. Solid* **2006**, *67*, 2065–2071. [CrossRef]
139. Lampakis, D.; Palles, D.; Liarokapis, E.; Kazakov, S.M.; Karpinski, J. Hydrostatic pressure induced phase separation in the $YBa_2Cu_4O_8$ superconductor. *J. Phys. Rev. B* **2005**, *72*, 014539. [CrossRef]
140. Osada, M.; Kakihana, M.; Käll, M.; Börjesson, L. Pressure-induced effects in high-Tc superconductors: Raman scattering as a probe of charge-lattice dynamics under high pressure. *Physica C* **2001**, *357–360*, 142–145. [CrossRef]
141. Liarokapis, E.; Lampakis, D.; Panagopoulos, C.; Nishizaki, T. High pressure study of Bi-2212. *High Press. Res.* **2003**, *23*, 111–115. [CrossRef]
142. Orenstein, J.; Millis, A.J. Advances in the Physics of high-temperature superconductivity. *Science* **2000**, *288*, 468–474. [CrossRef]
143. Lampakis, D.; Liarokapis, E.; Panagopoulos, C. Micro-Raman evidence for topological charge order across the superconducting dome of $La_{2-x}Sr_xCuO_4$. *Phys. Rev. B* **2006**, *73*, 174518. [CrossRef]
144. Liarokapis, E.; Lampakis, D.; Nishizaki, T.; Panagopoulos, C. Raman studies of the high pressure effects in high T_c superconductors. *High Press. Res.* **2000**, *18*, 109–116. [CrossRef]
145. Koch, U.; Lotter, N.; Wittig, J.; Assmus, W.; Gegenheimer, B.; Winzer, K. Pressure dependence of T_c for single crystal $YBa_2Cu_3O_{7-x}$ up to 10 GPa. *Solid State Commum.* **1988**, *67*, 959–963. [CrossRef]
146. Scholtz, J.J.; van Eenige, E.N.; Wijngaarden, R.J.; Griessen, R. Pressure dependence of T_c and H_{c2} of $YBa_2Cu_3O_8$. *Phys. Rev. B* **1992**, *45*, 3077–3082. [CrossRef] [PubMed]
147. Calamiotou, M.; Gantis, A.; Siranidi, E.; Lampakis, D.; Karpinski, J.; Liarokapis, E. Pressure-induced lattice instabilities and superconductivity in $YBa_2Cu_4O_8$ and optimally doped $YBa_2Cu_3O_{7-\delta}$. *Phys. Rev. B* **2009**, *80*, 214517. [CrossRef]
148. Karpinski, J.; Kazakov, S.M.; Angst, M.; Mironov, A.; Mali, M.; Roos, J. Influence of Sr substitution on the structure, charge distribution, and critical temperature of $Y(Ba_{1-x}Sr_x)_2Cu_4O_8$ single crystals. *Phys. Rev. B* **2001**, *64*, 094518. [CrossRef]
149. Calamiotou, M.; Gantis, A.; Lampakis, D.; Siranidi, E.; Liarokapis, E.; Margiolaki, I.; Conder, K. Pressure-induced phase separation in the Y123 superconductor. *Eur. Phys. Lett.* **2009**, *85*, 26004. [CrossRef]
150. Kenichi, T. Evaluation of the hydrostaticity of a helium-pressure medium with powder x-ray diffraction techniques. *J. Appl. Phys.* **2001**, *89*, 662–668.
151. Calamiotou, M.; Parisiades, P.; Siranidi, E.; Lampakis, D.; Conder, K.; Liarokapis, E. Pressure induced lattice effects in pure and near optimally doped $La_{2-x}Sr_xCuO_4$. *Physica C* **2019**, *565*, 1353516. [CrossRef]
152. Ohtani, T.; Himeda, Y.; Norimatsu, Y.; Akiyama, N. T_c increase of Bi2212 induced by exposure to organic liquids or by photocatalytic effect using TiO_2. *Bull. Okayama Univ. Sci.* **2016**, *52*, 35–44.
153. Raghuveer, V.; Thampi, R.; Xanthopoulos, N.; Mathieu, H.J.; Viswanathan, B. Rare earth cuprates as electrocatalysts for ethanol oxidation. *Solid State Ion.* **2001**, *140*, 263–274. [CrossRef]
154. Gupta, M.; Gupta, R. Pressure dependence of the hole concentration in superconducting $La_{1.85}Sr_{0.15}CuO_4$. *Physica C* **1991**, *173*, 381–386. [CrossRef]
155. Ganguly, P.; Shah, N.; Phadke, M.; Ramaswamy, V.; Mulla, I.S. Deviations from Vegard's law: Charges in the c-axis parameter in $La_{2-x}Sr_xCuO_{4-d}$ in relation to the insulator-superconductor-metal transition. *Phys. Rev. B* **1993**, *47*, 991–995. [CrossRef]